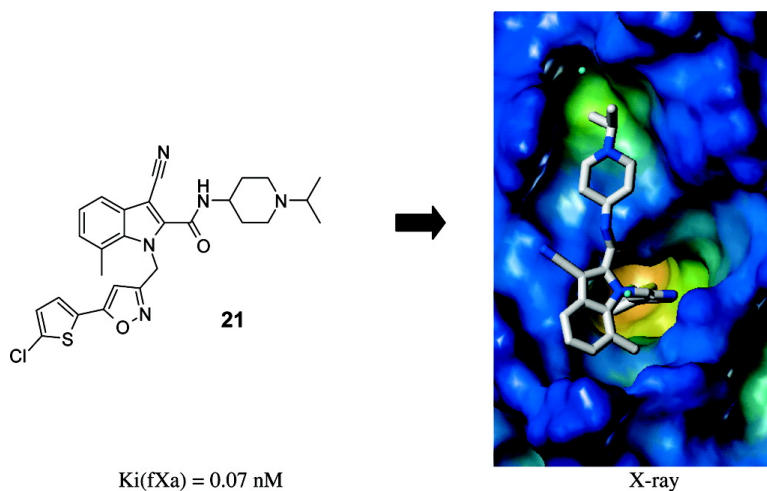


Probing the Subpockets of Factor Xa Reveals Two Binding Modes for Inhibitors Based on a 2-Carboxyindole Scaffold: A Study Combining Structure-Activity Relationship and X-ray Crystallography

Marc Nazar, David W. Will, Hans Matter, Herman Schreuder, Kurt Ritter, Matthias Urmann, Melanie Essrich, Armin Bauer, Michael Wagner, Jrg Czech, Martin Lorenz, Volker Laux, and Volkmar Wehner

J. Med. Chem., **2005**, 48 (14), 4511-4525 • DOI: 10.1021/jm0490540 • Publication Date (Web): 11 June 2005

Downloaded from <http://pubs.acs.org> on March 28, 2009



More About This Article

Additional resources and features associated with this article are available within the HTML version:

- Supporting Information
- Links to the 3 articles that cite this article, as of the time of this article download
- Access to high resolution figures
- Links to articles and content related to this article
- Copyright permission to reproduce figures and/or text from this article

[View the Full Text HTML](#)

Articles

Probing the Subpockets of Factor Xa Reveals Two Binding Modes for Inhibitors Based on a 2-Carboxyindole Scaffold: A Study Combining Structure-Activity Relationship and X-ray Crystallography

Marc Nazaré,* David W. Will, Hans Matter, Herman Schreuder, Kurt Ritter, Matthias Urmann, Melanie Essrich, Armin Bauer, Michael Wagner, Jörg Czech, Martin Lorenz, Volker Laux, and Volkmar Wehner
Aventis Pharma Deutschland GmbH, a company of the Sanofi-Aventis group, Industriepark Höchst, Building G878, D-65926 Frankfurt am Main, Germany

Received November 22, 2004

Structure–activity relationships within a series of highly potent 2-carboxyindole-based factor Xa inhibitors incorporating a neutral P1 ligand are described with particular emphasis on the structural requirements for addressing subpockets of the factor Xa enzyme. Interactions with the subpockets were probed by systematic substitution of the 2-carboxyindole scaffold, in combination with privileged P1 and P4 substituents. Combining the most favorable substituents at the indole nucleus led to the discovery of a remarkably potent factor Xa inhibitor displaying a K_i value of 0.07 nM. X-ray crystallography of inhibitors bound to factor Xa revealed substituent-dependent switching of the inhibitor binding mode and provided a rationale for the SAR obtained. These results underscore the key role played by the P1 ligand not only in determining the binding affinity of the inhibitor by direct interaction but also in modifying the binding mode of the whole scaffold, resulting in a nonlinear SAR.

1. Introduction

Thromboembolic diseases, including deep vein thrombosis, myocardial infarction, and pulmonary embolism, are major causes of mortality in Europe and North America.¹ Unfortunately the standard anticoagulants currently used for the treatment and prevention of these diseases have several disadvantages. These include slow onset of action, parenteral mode of administration, and severe, potentially life-threatening side effects such as excessive bleeding requiring stringent monitoring of drug levels.² The serine protease factor Xa (fXa) has emerged as an attractive target for the therapy of thrombosis-related diseases because it is a key enzyme in the activation cascade of the blood coagulation system, linking the extrinsic and intrinsic activation pathways.³ It is anticipated that inhibition of fXa should prevent thrombus formation without compromising normal hemostasis and platelet function by maintaining a basal thrombin level.⁴ An orally available fXa inhibitor should therefore be a superior antithrombotic agent and overcome the shortcomings associated with the current treatment. A major obstacle to the development of an orally available drug from the many potent and selective inhibitors available is often the requirement for a highly basic benzamidine or guanidine serving as an arginine mimetic in the S1 pocket of fXa. In general, these moieties are linked to the extremely poor bioavailability observed for the inhibitors bearing this functionality.⁵ Fortunately, recently a range of potent nonbasic fXa inhibitors has emerged, opening up exciting possibilities

for the development of orally bioavailable compounds without resorting to prodrug⁶ approaches. These compounds either contain nonbasic amidine isosteres, for example, razaxaban,⁷ or exploit the so-called chloro binding mode in the S1 pocket.⁸

In previous communications,⁹ we described 2-carboxyindole fXa inhibitors that carried the P1 ligand at the indole N1 and the P4 ligand as 2-carboxamides and that were otherwise undecorated. We described the optimization of various neutral P1 ligands using the chloro binding mode and piperidine-derived P4 ligands attached to the carboxyindole scaffold leading to a set of interchangeable P1 and P4 ligands and thus highly active inhibitors. The key primary interactions necessary for potent inhibition of fXa are those in the S1 and S4 pockets. The choice of ligands that provide optimal interactions within these pockets combined with a suitable scaffold ensuring the correct trajectories for the ligands has been a major focus in fXa inhibitor research.¹⁰ In most cases the scaffold is accommodated at the S3/S4 β -sheet region and acts as an amino acid mimetic with differing degrees of conformational constraint (Figure 1).

The indole scaffold is highly rigid compared to many other scaffolds. We believed that the lack of flexibility and adaptability of the indole scaffold could be a superior prerequisite for addressing secondary interactions. Although so far we had not exploited the possibilities of addressing subsites of the fXa enzyme by substituting the cyclic perimeter of the indole nucleus, we were intrigued by the potential for increasing binding affinity through interactions in this region. In addition, only a few reports have systematically ex-

* To whom correspondence should be addressed. Phone: +49(0)69 30515150. Fax: +49(0)69 331399. E-mail: Marc.Nazare@sanofi-aventis.com.

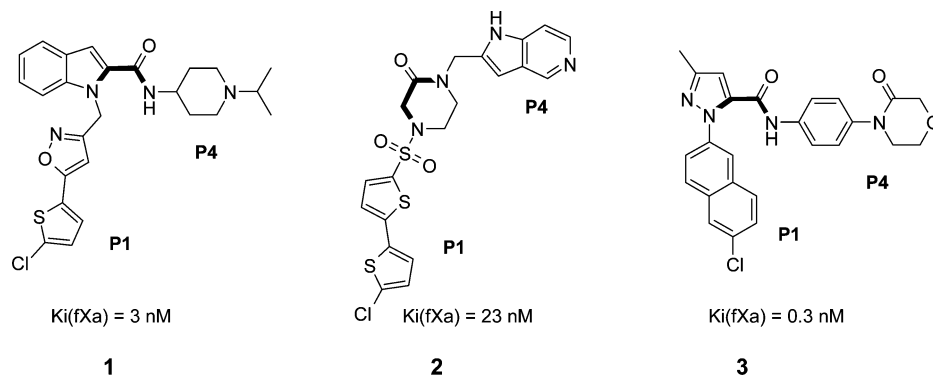
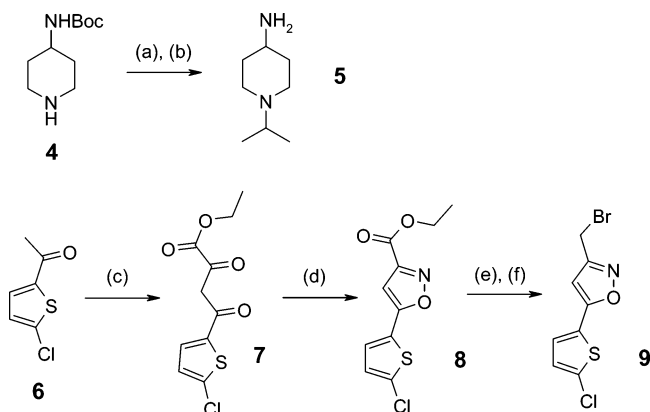


Figure 1. Highly potent fXa inhibitors **1**,⁹ **2**,¹¹ **3**¹² with amino acid mimetic scaffolds.

Scheme 1. Synthetic Routes to the P1 and P4 Ligands^a



^a Reagents and conditions: (a) acetone, NaBH_3CN , AcOH, methanol, room temp, 16 h, 80%; (b) HCl/MeOH, room temp, 16 h, 100%; (c) $\text{KO}^t\text{-Bu}$, then oxalic acid diethyl ester, toluene, room temp, 3 h, 62%; (d) $\text{NH}_2\text{OH}\cdot\text{HCl}$, ethanol, reflux, 6 h, 89%; (e) NaBH_4 , ethanol, room temp, 12 h, 67%; (f) NBS, PPh_3 (polystyrene-bound), CH_2Cl_2 , room temp, 1 h, 77%.

explored and elucidated by X-ray crystallography the opportunities of secondary interactions provided by means of scaffold substitutions.^{13,14} We intended, therefore, to explore the influence of various substituents and substitution patterns at the indole scaffold on the inhibition of fXa and to characterize the interactions using X-ray crystallography and molecular modeling. The inhibitors synthesized contained an optimal combination of P1 and P4 ligands, allowing us to probe the interplay of secondary interactions of the modified indole nucleus with the fXa protein, both in terms of inhibitory activity and through X-ray crystallography. Here, we report our findings on the effect of several substitution patterns resulting in a dramatic enhancement in binding affinity by specifically addressing subsites of the fXa enzyme, leading to a 0.07 nM¹⁵ inhibitor **21**, and provide a stringent analysis of key interactions based on X-ray crystal structures of inhibitor/fXa complexes.

2. Chemistry

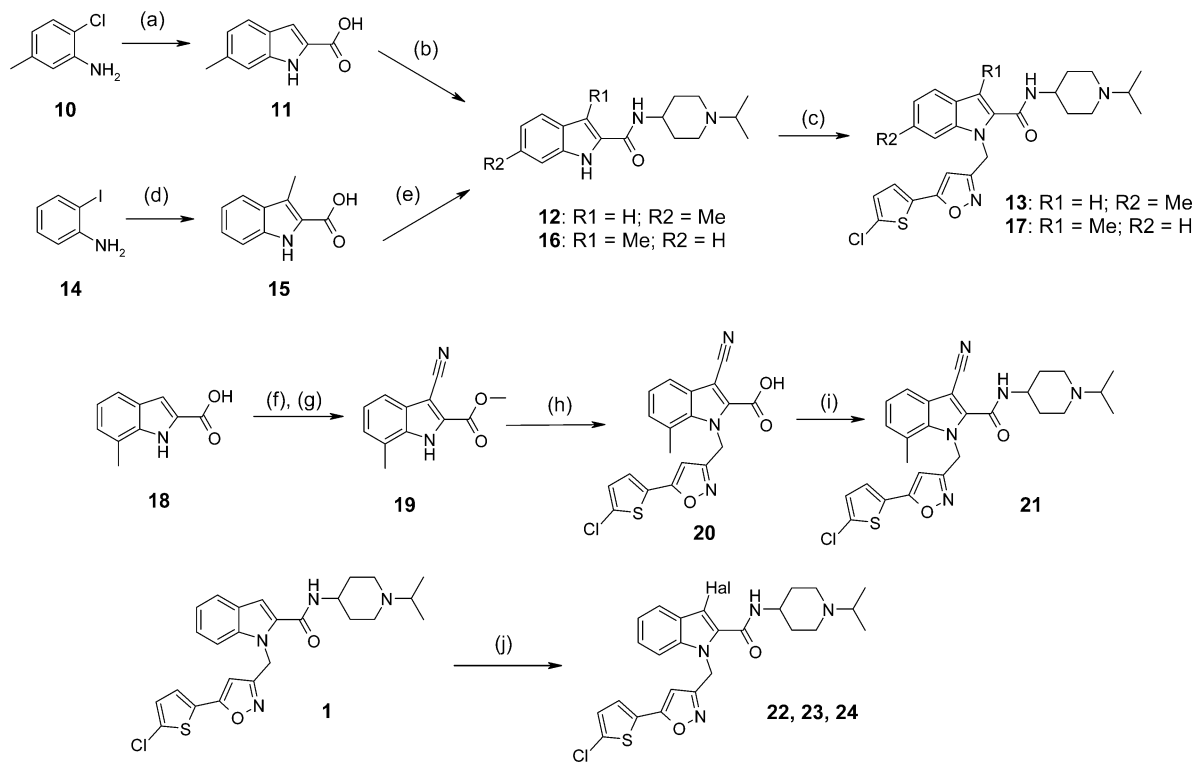
We first set out to systematically probe the influence on fXa activity of a diverse set of simple substituents on the indole nucleus. The biaryllic P1 ligand and the isopropylpiperidine P4 ligand were kept constant in this series of compounds and served as strong anchor points for the putative inhibitors. Scheme 1 illustrates the synthesis of the key P4 and P1 building blocks **5** and **9**

used throughout this investigation. The P4 ligand **5** was prepared from commercially available *N*-Boc protected 4-aminopiperidine **4** in two steps by reductive amination with acetone followed by acid-catalyzed removal of the Boc group. The biaryl bromide **9** was synthesized by condensation of 1-(5-chlorothiophen-2-yl)ethanone **6** with oxalic acid diethyl ester followed by regioselective formation of the isoxazole ring by treatment with hydroxylamine. Reduction of the ester in **8** and subsequent bromination yielded bromide **9**.

The benzo-substituted indole nuclei were either commercially available or readily accessible through standard indole synthesis procedures.¹⁶ Scheme 2 gives a representative illustration of key transformations for the synthesis of the substituted indole scaffolds, together with the two principal reaction sequences to attach the P1 and P4 ligands to give the fully decorated inhibitors. The 2-carboxy-6-methylindole scaffold **11** was synthesized by reaction of 2-chloro-5-methylaniline **10** with 2-oxopropionic acid under palladium catalysis.¹⁷ Inhibitor **13** was then assembled by amide coupling with **5** using TOTU, to give amide **12**, followed by *N*-alkylation of the indole with bromide **9** in the presence of sodium hydride. The 3-methylindole **17** was constructed employing a similar procedure, exemplifying the generality of this strategy. The use of 2-oxobutanoic acid allowed the introduction of the 3-methyl substituent directly during the annulation reaction to give compound **15**. The other pathway for constructing the fully decorated inhibitors is illustrated by the synthesis of compound **21**. 7-Methyl-2-carboxyindole **18** was converted into its methyl ester under standard conditions followed by selective iodination of the 3-position and palladium-catalyzed exchange with cyanide to yield **19**. This precursor was first alkylated with bromide **9** using sodium hydride, and after saponification to the acid **20**, amide coupling with **5** led to the desired compound **21**. All other compounds described were synthesized analogously.

The 3-chloro- and bromo-substituted inhibitors **23** and **24** were synthesized by selective halogenation of inhibitor **1** using *N*-chlorosuccinimide or *N*-bromosuccinimide, respectively. The 3-fluoroindole inhibitor **22** was synthesized analogously, using *N*-fluoropyridinium triflate.

Using these synthetic routes, we were able to systematically synthesize a wide range of fXa inhibitors and obtain dense SAR data that revealed several key features of favorable and unfavorable interactions.

Scheme 2. Synthetic Routes to Substituted Indole Scaffolds and Inhibitors^a

^a Reagents and conditions: (a) 2-oxopropionic acid, [Pd(*t*-Bu₃P)₂], K₃PO₄, AcOH, MgSO₄, DMA 140 °C, 44%; (b) **5**, TOTU, *N*-ethylmorpholine, CH₂Cl₂, room temp, 16 h, 59%; (c) **9**, NaH, DMF, 70 °C, 16 h, 15% for **13** and 10% for **17**; (d) 2-oxobutanoic acid, Pd(OAc)₂, DABCO, MgSO₄, DMF 105 °C, 55%; (e) **5**, BOP-Cl, NEt₃, CH₂Cl₂, room temp, 16 h, 99%; (f) HCl/MeOH, room temp, 16 h, 100%; (g) (i) I₂, DMF, room temp, 16 h, 94%; (ii) CuCN, Et₄NCN, dppe, Pd₂(dba)₃, DMF/THF, 120 °C, 5 h, 15%; (h) **9**, NaH, DMF, room temp, 16 h, then LiOH, THF/H₂O, 60 °C, 2 h, 39% two steps; (i) **5**, TOTU, *N*-ethylmorpholine, CH₂Cl₂, room temp, 16 h, 59%; (j) (i) Hal = F, *N*-fluoropyridinium triflate, CH₂Cl₂, room temp, 4 days, 50%; (ii) Hal = Cl, NCS, CH₂Cl₂, room temp, 16 h, 36%; (iii) Hal = Br, NBS, CH₂Cl₂, room temp, 16 h, 40%.

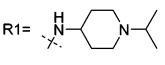
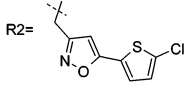
3. Results and Discussion

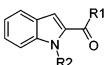
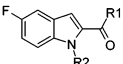
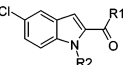
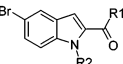
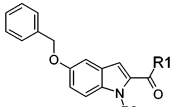
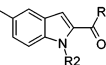
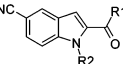
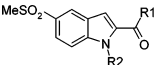
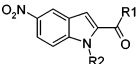
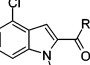
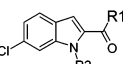
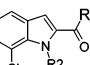
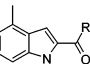
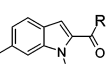
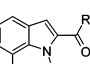
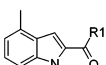
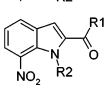
3.1. Structure-Activity Relationship at the Indole Scaffold. Table 1 shows the effect on fXa inhibitory activity of substitution at the benzo ring of the indole. The P1 and P4 ligands of the compounds in Table 1 were kept constant to allow the influence of the indole substitution to be observed in isolation. We first chose to investigate substitution at the 5-position of the indole because many of the starting materials were commercially available or easily accessible in high yield by standard indole synthesis. A fluoro substituent in this position (**25**) did not affect fXa binding affinity in comparison to the unsubstituted reference compound **1** ($K_i = 3$ nM). Increasing the size of the halogen (compounds **26–27**, $K_i = 5$ and 9 nM) reduced fXa binding affinity, and the introduction of a large benzyloxy substituent was extremely deleterious to affinity (**28**, $K_i = 835$ nM). The 5-methyl derivative **29** ($K_i = 9$ nM) was 3-fold less potent than **1**. Compounds **30–32** show the effect of increasing the polarity of the substituent at this site of the indole ring, with small polar moieties being most favorable at this position (**32**, NO₂ $K_i = 1$ nM) and the methylsulfone derivative **31** clearly being too large (20 nM). Introduction of a single chloro substituent at positions 4, 5, and 6 of the indole (compounds **26**, **33**, and **34**) resulted in a 2-fold loss in binding affinity compared to the unsubstituted reference compound **1**. The position of the chloro substituent had almost no influence on the potency of the compounds

in this series. Compounds **13**, **29**, **36**, **37**, with chlorine replaced by a methyl group with different steric and electrostatic properties, showed a different affinity pattern. The 4-methylindole **36** was equipotent to reference compound **1**, whereas compound **29** was 3 times less potent. Surprisingly the 6-methyl compound **13** with a K_i of 18 nM was the least active methyl-substituted derivative in this study. Most remarkably, the 7-methyl derivative **37**, with a K_i of 0.25 nM, was more than an order of magnitude more potent than **1**. Combining the substituents in the 4- and 7-position of compounds **36** and **37** to give dimethyl derivative **38** did not improve on the remarkable affinity of **37**. The most potent compound in this series was the 7-nitro derivative **39** ($K_i = 0.1$ nM), which, because of the presence of the undesirable nitro group, was not considered as a suitable druglike structure for further investigation. A comparison of the affinity of compounds **35** and **37** suggests that the chloro substituent ($K_i = 0.7$ nM) fits almost as well into the putative enzyme subpocket as the methyl substituent ($K_i = 0.25$ nM). The structural basis for the observed SAR was elucidated using X-ray crystallography of selected inhibitors complexed with fXa and will be discussed below.

3.2. Structure-Activity Relationship at the Indole 3-Position. The remarkable increase in fXa binding affinity resulting from introduction of an optimal substituent in the 7-position of the indole encouraged us to investigate substitution at the 3-position. The

Table 1. Substitution on the Benzo Ring of the Indole Scaffold

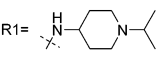
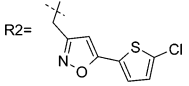
R1=  R2= 

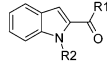
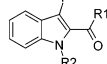
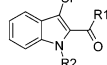
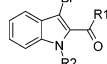
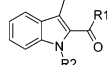
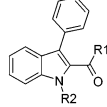
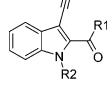
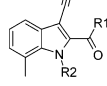
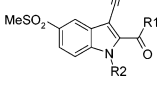
Compd	Indole	K _i (fXa) ^a nM
1		3
25		3
26		5
27		9
28		835
29		9
30		2
31		20
32		1
33		7
34		7
35		0.7
36		3
13		18
37		0.25
38		1
39		0.10

^a K_i values were measured as described in ref 15.

results are shown in Table 2. Introduction of lipophilic steric bulk in the form of halogen or methyl substituents (compounds **22–24**, **17**) did not influence potency significantly compared to the unsubstituted reference **1** (e.g., **23**, 3-Cl, K_i = 2 nM). Compound **40**, with a larger planar phenyl substituent was 18 times less potent than

Table 2. Substitution at the 3-Position of the Indole Scaffold

R1=  R2= 

Compd	Indole	K _i (fXa) ^a nM
1		3
22		2
23		2
24		2
17		3
40		55
41		0.30
21		0.07
42		7

^a K_i values were measured as described in ref 15.

1. Remarkably, the introduction of a nitrile moiety in the 3-position resulted in a 10-fold increase in fXa binding affinity, giving compound **41** with a K_i value of 0.3 nM. Combining the favorable interactions of the 7-methyl group used in compound **37** and the 3-nitrile group yielded the most active inhibitor **21** with a K_i value for fXa inhibition of 0.07 nM. The 3-nitrile substitution was also capable of compensating for less favorable substitutions such as methylsulfonyl **42**, which is approximately 3 times more potent than its parent compound **31**.

3.3. Exploring Alternative P1 Substituents. With this encouraging structure-activity relationship data in hand, we then intended to determine how general these interactions would be in the series and in particular if this substitution pattern would also display a superior fXa binding affinity in combination with other P1 ligands. Table 3 shows the results for a set of six 2-carboxyindole fXa inhibitors, containing three different P1 ligands and that are, in each case, unsubstituted at the indole core or contain the 3-cyano,7-methyl substitution pattern that was found to be optimal in combination with the biaryl P1 ligand.

Surprisingly the attempt to transfer the optimal indole substitution pattern led to compounds that were significantly less active than the initial unsubstituted ones. For example, when combined with the *m*-methoxybenzyl P1 ligand in **44**, a 4-fold drop in activity was

Table 3. Effect of 3-Cyano,7-Methyl Substitution of the Indole Scaffold in Combination with Different P1 Ligands

Compd	Structure	K _i (fXa) ^a nM
1		3
21		0.07
43		89
44		406
45		3
46		26
47		25

^a K_i values were measured as described in ref 15.

observed compared to the unsubstituted compound **43** (K_i = 406 vs 89 nM). Even more remarkable was the 6-fold loss in activity in conjunction with the 4-chlorophenylacetamide as the P1 ligand (**46** K_i = 26 nM vs **45** K_i = 3 nM). This unexpectedly divergent SAR behavior strongly suggested that the inhibitors in Table 3 with different P1 ligands have different binding modes to the fXa enzyme and emphasized the dominance of the P1 ligand interaction with fXa.

3.4. Binding Modes of Indoles with Biaryl P1 Substituents. These conflicting SAR observations and the exceptional binding affinity of the 3-cyano,7-methyl derivative **21** with a chlorobiaryl P1 substituent prompted us to investigate the binding modes of selected derivatives by X-ray crystal structure analysis of their complexes with fXa.

We obtained four X-ray crystal structures of factor Xa with compounds **1** (K_i = 3 nM), **21** (K_i = 0.07 nM), **43**

Table 4. Data Collection and Refinement Statistics for Five Factor Xa X-ray Structures

	inhibitor				
	1	21	43	45	47
detector	ID14-1 ^a	mar345	mar345	mar300	mar300
space group	P2 ₁ 2 ₁ 2 ₁	P2 ₁ 2 ₁ 2 ₁	P2 ₁ 2 ₁ 2 ₁	P2 ₁ 2 ₁ 2 ₁	P2 ₁ 2 ₁ 2 ₁
cell dimensions					
<i>a</i> , Å	56.1	55.40	55.94	56.38	56.3
<i>b</i> , Å	72.0	70.65	72.05	71.90	72.0
<i>c</i> , Å	79.2	76.27	78.55	78.63	78.3
obsd refls	72 973	18 168	73 686	33 430	45 424
unique refls	16 670	5984	15 828	6939	12 329
resolution, Å	2.2	3.0	2.2	2.95	2.4
R _{sym} , %	7.9	7.2	5.1	10.3	6.7
completeness	98.8	94.0	94.8	97.4	95.2
protein atoms	2249	2240	2240	2240	2249
inhibitor atoms	33	36	30	32	32
calcium ions	1	1	1	1	1
water molecules	221	73	290	126	291
R-factor, %	20.7	20.2	21.8	18.4	18.1
R-free, %	25.3	29.8	27.2	26.1	28.0
rmsd bond lengths, Å	0.009	0.008	0.009	0.009	0.008
rmsd bond angles, deg	1.51	1.29	1.30	1.58	1.46
rmsd dihedrals, deg	25.2	24.0	24.5	24.3	24.7
rmsd impropers, deg	0.75	0.78	0.72	0.67	1.90

^a Beam line ID14-1 at the European Synchrotron Radiation Facility (ESRF).

(K_i = 89 nM), and **45** (K_i = 3 nM). In addition, one previous structure of an indole-2-carboxamide with an *m*-benzamidine in S1 was also used for analysis (PDB ID code 1lqd, **47**¹⁸). All crystals diffracted reasonably well with resolutions between 2.2 and 3.0 Å (see Experimental Section, Table 4). In general, the inhibitor binding modes are well-defined. Thus, the 2.2 Å structures are accurately defined, while the 3.0 Å structure is sufficiently accurate to indicate the binding mode.

While many first-generation fXa inhibitors rely on the interaction of a basic amidine with Asp189 at the bottom of the S1 pocket, these structures indicate favorable nonbasic interactions with residues in this subsite. Collectively these X-ray structures reveal that the chlorothiophene, chlorophenyl, or *m*-methoxyphenyl substituents are accommodated in S1. However, different interaction patterns for chloro or methoxy substituents were identified.

We will start our discussion with the X-ray structure of the unsubstituted reference compound **1** (K_i = 3 nM 2.2 Å) to rationalize the structure-activity relationship in this series. Its overall binding mode in factor Xa is shown in Figure 2. While Figure 2A summarizes key interactions of **1** with important amino acids, the detailed binding mode is shown in parts B–D of Figure 2. The protein binding site in Figure 2B,D is displayed as a solvent-accessible surface with cavity depth mapped onto it. Orange parts indicate the very deep and buried S1 pocket, while green and cyan parts refer to more shallow and solvent-exposed subsites, such as the S4 and EBP (“ester binding pocket”). Here, the protease S2 pocket is present as a small, solvent-exposed subsite inaccessible for inhibitors because of the aromatic Tyr99 separating S4 from S2.

Although the electron density of compound **1** is well-defined, the indole benzo ring and the S4 isopropyl moiety reveal a weaker density, which points to some disorder or conformational mobility in those parts filling the solvent-exposed regions of S4 and EBP.

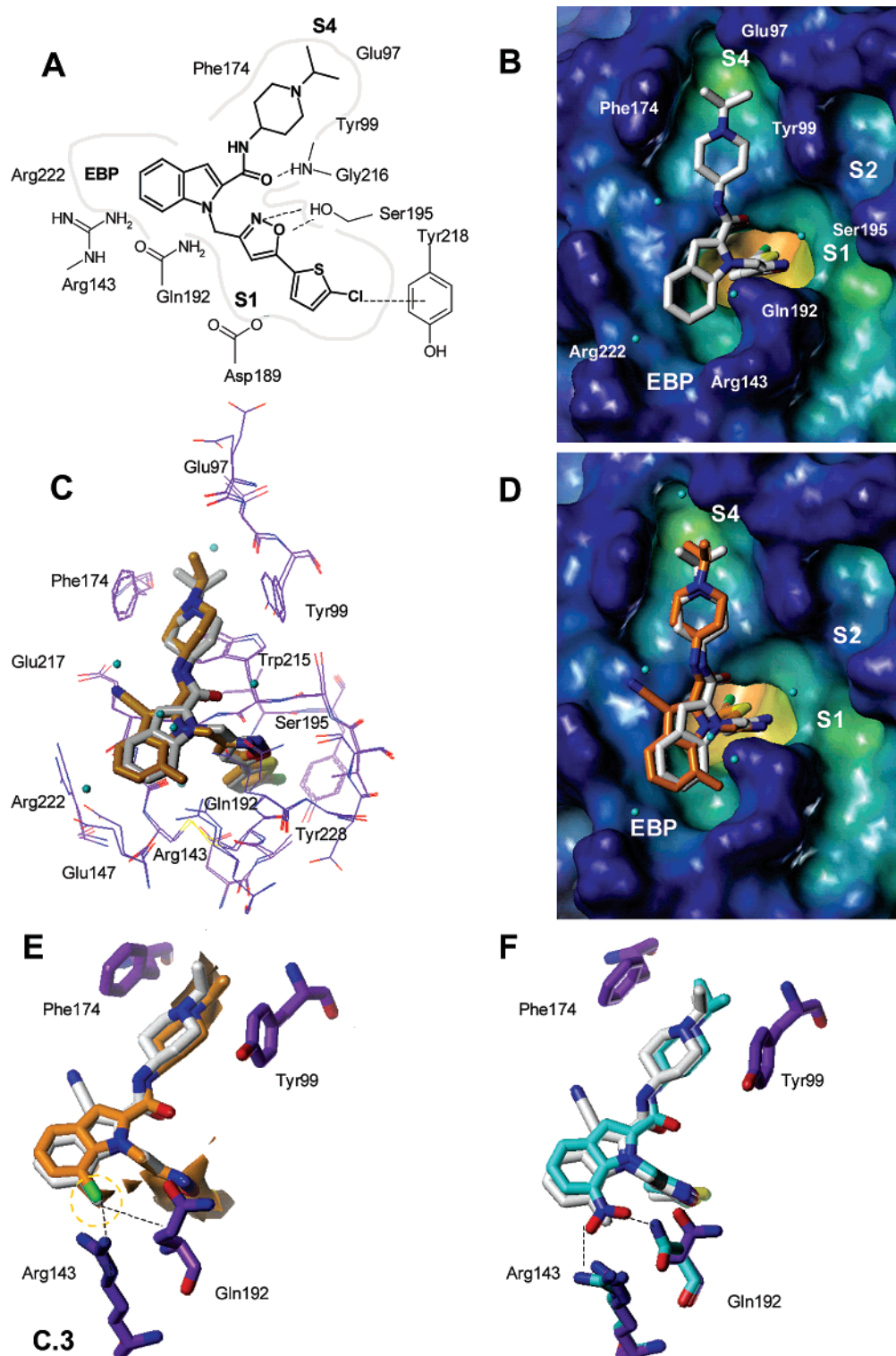


Figure 2. A 2.2 Å X-ray crystal structure of indole-2-carboxamide **1** ($K_i = 3$ nM) in complex with human fXa. (A) Schematic view of essential intermolecular interactions. (B) Binding mode with fXa shown as solvent-accessible surface color-coded by cavity depth (from orange to blue). Essential pockets are indicated as S1, S2, S4, and EBP (ester binding pocket). Structurally conserved water is displayed with cyan spheres. Essential amino acids are indicated. (C) Comparison of X-ray derived binding modes for **1** ($K_i = 3$ nM, white carbons) and **21** ($K_i = 0.07$ nM, orange carbons) with the P1 biaryl substituent in complex with factor Xa. (D) Same as (C) but with fXa solvent-accessible surface indicated. (E) Detailed analysis of the binding site from the fXa/**21** complex (white carbons) for favorable interactions with a GRID methyl probe (orange contours). Only key amino acids surrounding the EBP are shown. The favorable contour is highlighted using an orange circle. Key lipophilic contacts to Arg143 and Gln192 side chains are indicated and shown as dotted lines. In addition, the best docking mode for **35** ($K_i = 0.7$ nM, orange carbons) is indicated. (F) Comparison of the fXa/**21** (ligand with white carbons, protein with purple carbons) and best docking mode for **39** (ligand and protein with cyan carbons). Polar interactions of the 7-NO₂ group with fXa side chains are indicated.

The chlorothiophene substituent of **1** and related molecules is deeply buried inside the S1 pocket with the

chloro atom pointing toward the center of the Tyr228 aromatic ring. This atom replaces a structurally con-

served water molecule present in benzamidine-containing factor Xa structures. It is engaged in a lipophilic contact to the aromatic ring of Tyr228 with distances of 3.43–4.52 Å to the aromatic carbons and 3.76 Å to the ring centroid, in agreement with interaction data from force field methods such as GRID, which consistently predict a region of favorable interaction to Cl at the bottom of this pocket (see Figure 2F). The carbon–chlorine bond is directed toward the plane of the Tyr228 ring (dihedral angle C–Cl⋯Tyr228_(centroid)–Tyr228_(C_z): 118°). Additional details are obvious from inspection of Figure 2C, where **1** (white carbons) and **21** (orange carbons, $K_i = 0.07$ nM) are superimposed. This binding mode of chlorine in S1 is similar to that previously described for 3-oxybenzamides with a dichlorophenyl substituent in S1.^{13,14} This “chloro-binding mode” has been described by different groups for thrombin¹⁹ and fXa,^{8,14} indicating that electrostatic interactions between a benzamidine and Asp189 in S1 are not mandatory for high affinity. The thiophene sulfur atom is engaged in close contact with Val213-C γ (3.40 Å) and Trp215-C α (3.59 Å) lining the S1 pocket, while its carbon atoms are oriented toward the Asp189 side chain at the bottom of S1 (3.31–3.47 Å to Asp189-O γ 1 and -O γ 2). The isoxazole group is situated close to the active site Ser195-O γ , allowing reasonable hydrogen bonds to be formed between the O γ and both the isoxazole nitrogen (3.23 Å) and oxygen (3.04 Å) atoms (cf. Figure 2A and Figure 4E). Profiling the ligand **1** using the GRID force field and a hydrogen bond donating probe like amide NH or phenolic OH suggests, however, that the isoxazole nitrogen is a better hydrogen bonding acceptor. The isoxazole carbon is oriented toward Gly219-C=O (4.15 Å). Replacing the isoxazole ring by an amide, as in **45**, results in a short hydrogen-bonding interaction between the ligand amide NH group and Gly219 (2.91 Å), while interaction with Ser195 is no longer possible (C=O⋯O γ : 4.70 Å). This may imply the involvement of a structurally conserved water, although this is not detected in the X-ray structure.

No other direct hydrogen bonds were observed between factor Xa and **1**. The indole-2-carboxamide carbonyl oxygen is 3.65 Å from the Gly216-N, which is probably too long for a significant interaction. Again, a structurally conserved water molecule bridging both partners could be postulated here. The twist between the planes of the indole and amide groups is 25°. The isopropylpiperidine substituent is bound in the S4 pocket, surrounded by aromatic residues Phe174, Tyr99, and Trp215 at the bottom of the S4 pocket. Hydrophobic interactions are dominant in this pocket, but basic nitrogen atoms are also accommodated on top of the Trp215 ring system, as present in this and related structures. In contrast to the X-ray structures of 3-oxybenzamides with a 4-pyridylpiperidine substituent,¹⁴ the basic pyridyl nitrogen is missing here. Hence, no polar interaction with the network of hydrogen-bonding acceptors at the edge of this pocket or structurally conserved water is possible.

The indole benzo ring is situated on top of the Cys191–Cys220 disulfide bridge forming the bottom of the so-called “ester binding pocket” (EBP).¹³ This pocket is lined by the flexible side chains of the fXa residues Gln192, Arg143, and Glu147. The electron density of

both the Gln192 side chain and the indole is weak, which indicates some flexibility in this region. Inspection of Figure 2B also reveals an unoccupied subpocket between indole C7 and the aliphatic part of the Gln192 side chain.

In Figure 2C,D the binding mode of **1** (white carbons) is compared with the X-ray structure of the most active inhibitor **21** ($K_i = 0.07$ nM, orange carbons). The latter structure with a resolution of 3.0 Å provided additional insights into favorable interactions of both the 7-methyl and 3-nitrile groups. The hydrophobic 7-methyl group now fills the space between the indole C7 atom and the aliphatic portion of the Gln192 side chain. This flexible side chain is reoriented compared to its position in the fXa/**1** complex (distance Gln192-C δ 1.92 Å) and is in lipophilic contact with the methyl substituent (distance of 7-CH₃ group to Gln192-C β is 3.81 Å). This favorable contribution of a methyl carbon to binding affinity is in agreement with the analysis of favorable binding site interactions using GRID (cf. Figure 2E). Lipophilic contacts between the alkyl part of the Gln192 side chain and this methyl group or a chlorine atom contribute favorably to binding affinity (**35** 0.7 nM vs **37** 0.25 nM), as can be seen from the superimposition of the experimental binding mode of **21** in comparison to the best docking mode of **37** (orange carbons) in Figure 2E. From docking studies it can be concluded that the chlorine substituent in position 7 of the indole system also occupies this small subpocket and is able to interact via lipophilic contacts to both amino acid side chains. Moreover, the addition of a hydrogen bond acceptor to the indole-C7 position additionally favors binding affinity because of the surrounding hydrogen bond donors from the flexible Arg143 and Gln192-N ϵ H₂ side chains (e.g., distance C7–Gln192-N ϵ is 2.75 Å in the fXa/**1** complex). This is in good agreement with the remarkably high affinity of compound **39** ($K_i = 0.10$ nM) having an NO₂ substituent in this position. The best docking mode of **39** is shown in Figure 2F (cyan carbons) in comparison to the experimental fXa/**21** complex. Because all docking studies were carried out using flexible key residues, the side chains of Gln192 and Arg143 (cyan carbons in Figure 2F) move in order to undergo the proposed polar interaction with the NO₂ group **39** in this subpocket.

Interestingly, dimethyl substitution at positions 7 and 4 of the indole system results in reduced affinity compared to the 7-monomethyl substitution (**38** $K_i = 1$ nM vs **37** $K_i = 0.25$ nM). Because the 7-methyl substitution causes a minor shift of the indole scaffold within the EBP toward Arg222, the reduced affinity can be attributed to the closer contact between any bulky C4 substituent and the Arg222 guanidine (distance C4–Arg222-N ϵ of 4.34 Å in the fXa/**21** complex). The inhibitor with the same 4-methyl group but without 7-substitution does not undergo this slight shift in the EBP and thus shows the same binding affinity as its 7-unsubstituted derivative (**36** $K_i = 3$ nM vs **1** $K_i = 3$ nM). Substitutions at the indole 5-position also reduce affinity because of less favorable steric contacts to amino acids at the edge of the EBP, namely, the Arg222 side chain and the backbone carbonyl group of Glu147 (distances C5–Arg222-N ϵ of 4.44 Å and C5–Glu147-C=O of 3.80 Å in the fXa/**1** complex).

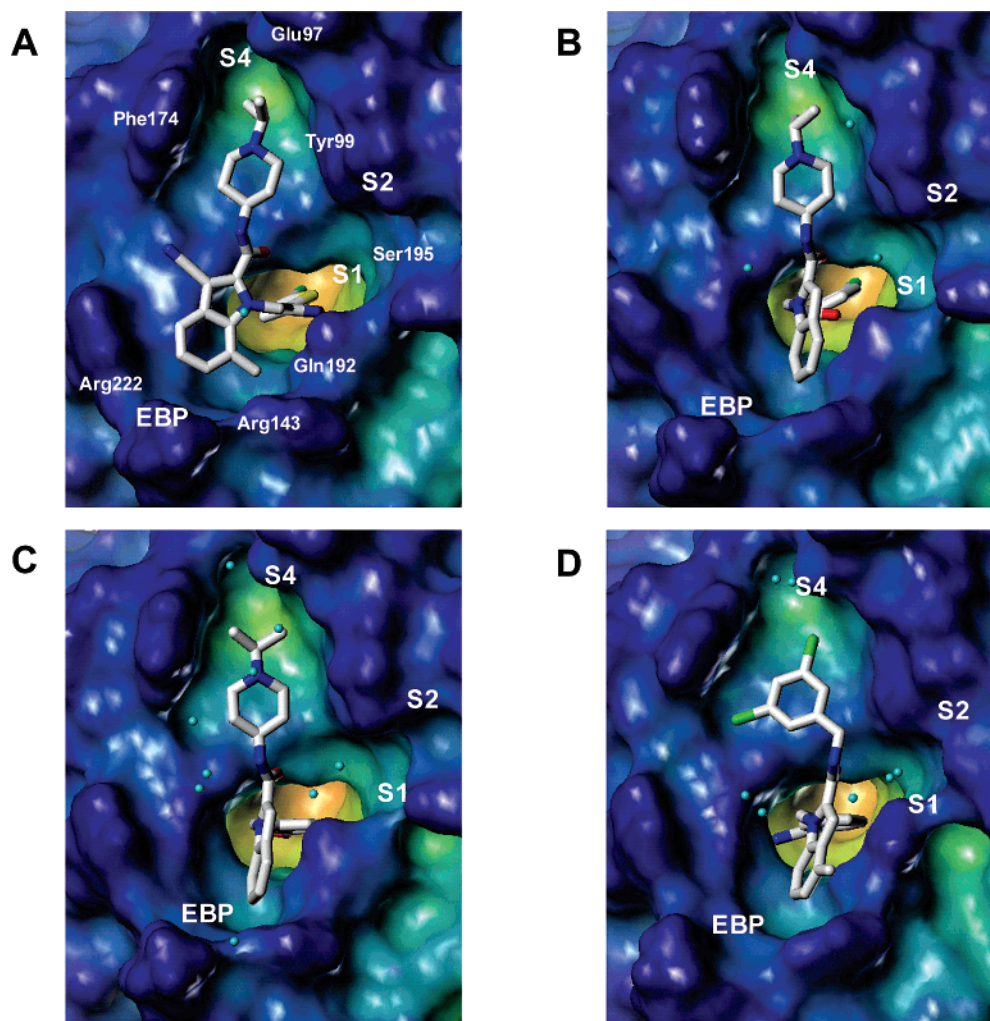


Figure 3. Comparison of X-ray binding modes for different indole-2-carboxamides in complex with human factor Xa. The following compounds are shown: (A) **21** (0.07 nM), (B) **45** (3 nM), (C) **43** (89 nM), (D) **47**¹⁸ (25 nM). The experimental factor Xa binding site is shown as a solvent-accessible surface color-coded by cavity depth (from orange to blue). Structurally conserved water is displayed as cyan spheres.

The 3-cyano substituent is oriented on top of the Glu217-C α atom (3.59 Å) close to the position of a structurally conserved water in the fXa/**1** complex (2.03 Å), which has been replaced in the fXa/**21** complex. Profiling ligand **21** using a GRID C.3 probe additionally suggests that this cyano substituent is involved in favorable interactions with aliphatic carbons, such as Glu217-C α . This cyano group with a larger dipole moment has a positive effect on binding affinity, shown by comparing the unsubstituted derivative **1** (K_i = 3 nM) with **41** (K_i = 0.30 nM). Its nitrogen atom with a partial negative charge is close to the C α carbon of Glu217 (3.59 Å) and its attached H α (2.63 Å), which both are more positively charged. Furthermore, the guanidine of the neighboring Arg222 creates a more positive electrostatic field in this region. Analysis using GRID and an sp nitrogen with lone pair indeed indicates favorable interactions in this area close to the cyano group. Obviously this electrostatic complementarity contributes positively to the fXa binding affinity because shorter and/or less charged substituents such as 3-methyl, chloro, and bromo are less potent fXa inhibitors with K_i values of 3 nM (**17**), 2 nM (**23**), and 2 nM (**24**) in comparison to **41** (K_i = 0.30 nM). Furthermore, the longer cyano substituent is directly situated on the

surface of the binding site and thus also increases affinity by two favorable contacts. The final effect contributing to fXa binding affinity originates from an enhanced twist of the indole-2-carboxamide dihedral angle from 25° to 46° caused by the sterically more demanding indole 3-substitution. Although this leads to a strained ligand geometry, its overall contribution for binding affinity is positive because an additional hydrogen bond between the amide C=O and Gly216-NH is formed (3.41 Å).

3.5. Binding Modes of Indoles with Other P1 Substituents. To understand the nonlinear structure-activity relationship upon transfer of the indole 3-cyano,7-methyl substitution pattern from **21** to different S1-directed substituents (Table 3), the X-ray crystal structure of fXa complexed with **45**, carrying a 4-chlorophenylacetamide substituent directed toward S1, was solved (resolution 2.95 Å, K_i = 3 nM). The reasonably strong electron density of inhibitor **45** is clear, although the position of the terminal S4 isopropyl is less well-defined and a mixture of conformations may be present, which may explain why a different rotamer was fitted at this position compared to the fXa/**1** complex.

In Figure 3 the binding modes for indole-2-carboxamide based inhibitors **21**, **45**, **43**, and **47**¹⁸ in fXa,

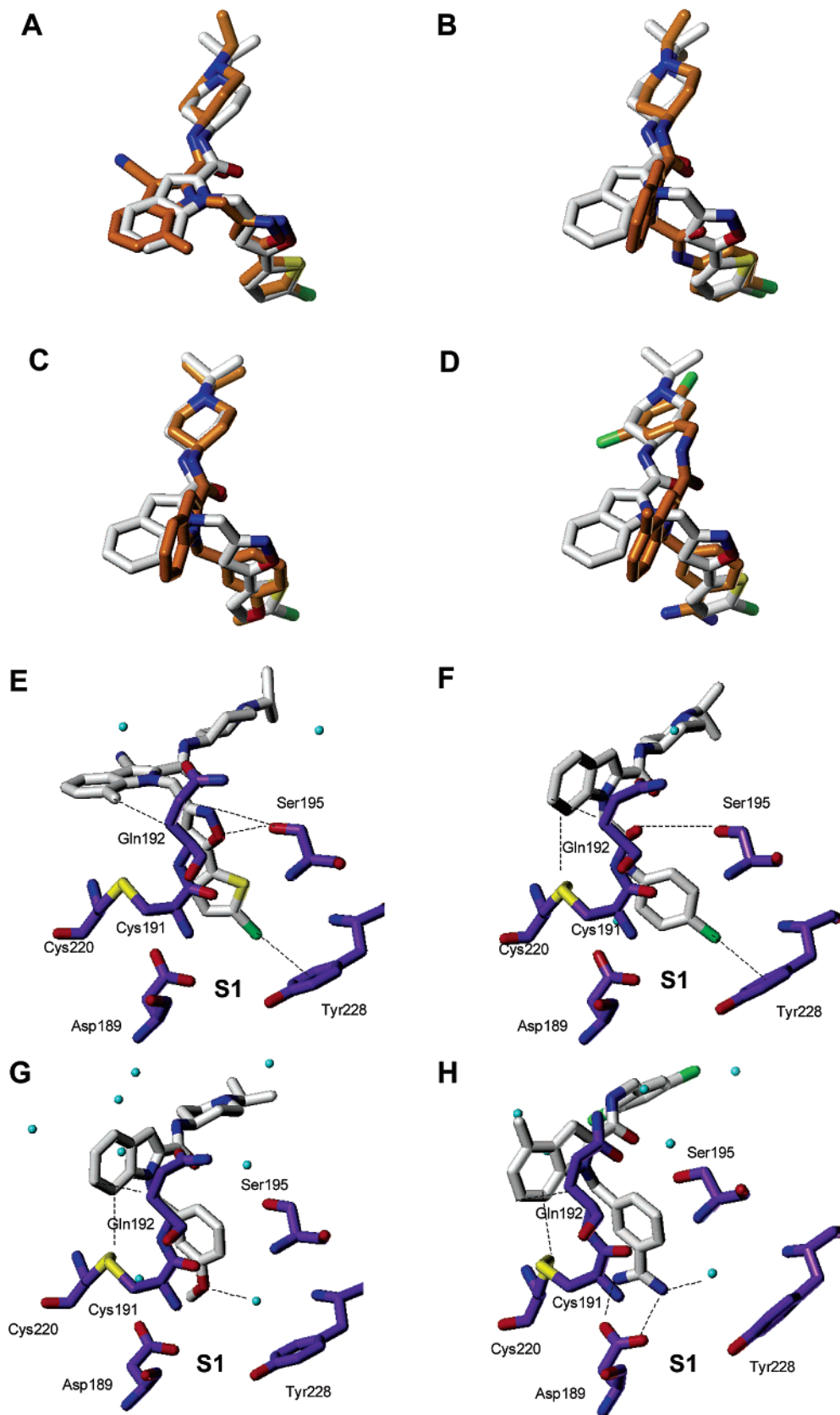


Figure 4. Superpositions of experimentally derived inhibitor binding modes from Figure 3 (orange carbons) with compound **1** (white carbons) from the crystal structure of its complex with human factor Xa. All superpositions are shown without protein binding sites (A–D). For comparison, each individual ligand is additionally displayed with key amino acids highlighted and with a focus on the factor Xa S1 pocket plus important interactions highlighted (E–H): (A, E) **21** (0.07 nM); (B, F) **45** (3 nM); (C, G) **43** (89 nM); (D, H) **47¹⁸** (25 nM).

indicated by the binding site solvent-accessible surfaces and cavity depth for color coding, are compared. The

superposition of these inhibitor binding modes (orange carbon atoms) onto the fXa/**1** complex is shown in Figure

4A–D (white carbons). This superposition was done using rms fitting of the entire protein domain, while only essential amino acids in S1 are displayed in Figure 4E–H.

The chlorine atom of the 4-chlorophenylacetamide moiety in **45** is situated 0.55 Å deeper in S1 compared to the fXa/**1** complex; its distance to the Tyr228 ring centroid is reduced to 3.44 Å. The acetamide nitrogen is at a distance of 2.84 Å from the backbone Gly219-C=O, suggesting a positive contribution from this hydrogen bond. It causes the acetamide carbonyl oxygen to be 4.59 Å away from the O γ atom of Ser195, which was interacting with the isoxazole ring in the biaryl-P1 substituent in **1**. Surprisingly, the orientation of the indole scaffold in **45** with this P1 substituent is perpendicular to the binding mode of indole-2-carboxamides with biaryl substituents. The binding mode of the isopropyl piperidine in S4 is, however, similar to that in the fXa/**1** and fXa/**21** complexes.

While Figures 2 and 4A,E demonstrate the similar binding modes for the biaryl compounds **1** and **21**, other P1 substituents led to a significant change of the indole orientation. Detailed inspection of Figures 3B and 4B,F for the fXa/**45** complex reveals the indole C7 atom in its perpendicular orientation to be in close contact with the Cys191–Cys220 disulfide bridge (C7–Cys220-S γ of 3.92 Å; C7–Cys191-S γ *o* ϕ 4.22 Å) at the bottom of the EBP. The neighboring C6 indole atom is involved in close contacts to Gln192-C β (3.56 Å) and to the carbonyl oxygen of Glu147 (3.74 Å), while the indole C5 carbon is close to the flexible side chain of Arg143 (e.g., to the guanidine carbon, 3.61 Å). The entire indole benzo ring plane is thus packed against the aliphatic part of the shifted Gln192 side chain. This binding mode now orients the indole C3 and C4 positions toward the solvent. It allows the 2-carboxyamide oxygen to be engaged in a hydrogen bond with Gly216-NH (3.37 Å), with a dihedral angle of –37.1° between the indole and amide planes. These changes in binding mode and significant interactions collectively contribute to the observed binding affinity of 3 nM for **45**. Interestingly, in all structures the isopropylpiperidine moiety is consistently situated in the S4 pocket between Tyr99, Phe174, and Trp215 without conformational changes.

The X-ray structure of **43** from the *m*-methoxybenzyl P1 series ($K_i = 89$ nM) was solved to a resolution of 2.2 Å. The electron density of the inhibitor is clear, its binding mode similar to the fXa/**45** complex with a perpendicular orientation of the indole scaffold (cf. Figures 3C and 4C,G). The *m*-methoxyphenyl group is located in S1 with its aromatic carbons at positions similar to positions of the corresponding benzamidines (e.g., **47**,¹⁸ Figures 3D and 4D,H). The oxygen atom is involved in a hydrogen bond to a structural water molecule (3.00 Å), which in turn is hydrogen-bonded to both the backbone nitrogen and carboxyl oxygen of Ile227 with distances of 3.41 and 3.08 Å, respectively (cf. Figure 4C,G). The methoxy oxygen atom is also close to the carbonyl oxygen of Ala190 (3.44 Å). As can be seen from Figure 4G, the carbon of the methoxy substituent points toward Asp189 at the bottom of S1 (2.93 and 3.17 Å). Both carboxylate oxygens of Asp189 are also involved in hydrogen bonds: one with bound water

molecules and one with the backbone nitrogens of Ala190 and Ala221, respectively. The observation that the methyl group points toward Asp189 (Figure 4G) could possibly be explained by the involvement of both Asp189 carboxylate oxygens in two hydrogen bonds each, one with a bound water molecule and one with the backbone nitrogens of Ala190 and Ala221. Thus, no unsatisfied hydrogen-bonding partners are left in S1.

Because of a slight movement (~ 0.5 Å) of the structurally conserved water in the S1 pocket, together with a small rotation of the benzene ring, both benzamidine and methoxyphenyl moieties are able to form a good hydrogen bond with the bound water molecule, as indicated in Figure 4G,H, which may explain the observed binding affinity of these compounds.

These different indole orientations of **43** and **45** in complex with fXa compared to **1** suggest that any substituent attached to the aromatic C7 carbon affects this binding mode and results in a reduced affinity in comparison with unsubstituted analogues. This is in perfect agreement with the SAR of the *m*-methoxybenzyl P1 series with a 4-fold reduction of affinity for the corresponding 3-cyano,7-methyl derivative **44** ($K_i = 406$) versus the unsubstituted derivative **43** ($K_i = 89$ nM). It also agrees with the experimental observations for the 4-chlorophenylacetamide P1 series with the corresponding 3-cyano,7-methyl derivative **46** ($K_i = 26$ nM) compared to the unsubstituted compound **45** ($K_i = 3$ nM). Again, the perpendicular orientation of the indole scaffold explains the reduced binding affinity by introducing substituents into the indole C3 and C7 positions. Hence, the divergent SAR of the compounds shown in Table 3 is explained by differing binding modes of the central scaffold, depending on the nature of the P1 substituent.

Finally, the binding mode of **47**¹⁸ with a 3-amidinobenzyl substituent attached at the indole N1 indicates that this substituent is located in the S1 pocket and interacts with Asp189 at the bottom of this pocket (cf. Figures 3D and 4D,H). This is the typical binding mode observed for other benzamidine-based factor Xa inhibitors. The indole scaffold itself is solvent-exposed and stacked upon the flexible side chain of Gln192. This orientation is similar to that observed for compounds **43** and **45** with the indole C7 in van der Waals contact to the Cys191–Cys220 disulfide bond at the bottom of the EBP. For compound **47**, the terminal dichlorobenzyl substituent is oriented almost parallel to the aromatic side chain of Trp215 at the bottom of S4 and perpendicular to the rings of Tyr99 and Phe174. The two Cl atoms attached to the benzyl ring in this pocket have strong electron density. Cl-1 points deep into the S4 pocket, while Cl-2 points toward the solvent and in the direction of Glu217. Hence, all alternative P1 motifs except the biaryl substituent result in this perpendicular indole orientation, while this rigid moiety provides an ideal topology to orient the indole scaffold in a position optimally suited to access previously unoccupied pockets of the factor Xa binding site by additional substituents. This finding offers many possibilities for further design of potent fXa inhibitors with neutral P1 substituents.

4. Conclusion

In this study we have explored the SAR of a series of 2-carboxyindole factor Xa inhibitors by systematic sub-

stitution at all positions of the indole scaffold. Addressing subpockets in the enzyme, such as the EBP with suitable substituents, which allowed additional lipophilic and hydrogen-bonding interactions, resulted in a significant improvement in binding affinity. Furthermore, combination of optimal substituents resulted in an even more dramatic increase in potency. The 3-cyano,7-methyl substitution pattern was found to be an optimal arrangement in combination with the chlorothienylisoxazole P1 moiety and the 4-isopropylpiperidine P4 portion (**21**, $K_i = 0.07$ nM). Surprisingly this substitution pattern was deleterious when combined with a 4-chloroanilinetamide or an *m*-methoxybenzyl P1 ligand. This divergent SAR behavior is explained by X-ray crystallographic analysis of fXa/inhibitor complexes. It became apparent that, in contrast to analogous P1-benzamidine-containing inhibitors, the chlorothienylisoxazole P1 ligand induced an unexpected 90° rotation of the indole scaffold, making the subpockets identified accessible with this alternative binding mode. The inhibitors with 4-chloroanilinetamide or *m*-methoxybenzyl P1 ligands displayed the upright positioning of the indole core described previously for analogous P1-benzamidine-containing inhibitors, and thus, the 3-cyano,7-methyl substitution pattern resulted in unfavorable interactions. Another surprising feature of this inhibitor series is that the 4-isopropylpiperidine P4 ligand was capable of mediating the required interactions in the S4 pocket for both binding modes. These results underscore the key role played by the P1 ligand not only in determining the binding affinity by direct interaction of its neutral chlorine atom to the aromatic ring of Tyr228 but also in modifying the binding mode of the entire scaffold, resulting in a nonlinear SAR. Exploiting this behavior may potentially allow the generation of other highly potent fXa inhibitors with novel P1-ligand-scaffold combinations.

5. Experimental Section

5.1. Chemistry. Solvents and other reagents were used as received without further purification. Column chromatography was carried out on Merck silica gel 60 (230–400 mesh). Reversed-phase high-pressure chromatography was conducted on a Abimed Gilson instrument using a LiChrospher 100 RP-18e (5 μ m) column from Merck. Thin-layer chromatography was carried out on TLC aluminum sheets with silica gel 60F254 from Merck. LC-MS analyses were performed on an Agilent series HP1100 system using a YMC J sphere ODS H80 20 mm \times 2.1 mm (4 μ m) column and a Merck Purosphere 55 mm \times 2 mm (3 μ m) column or on a Waters 2790 HPLC, using a Waters Symmetry C18, 50 mm \times 2.1 mm (3.5 μ m) column. Varying ratios of acetonitrile and 0.05% trifluoroacetic acid or 0.1% formic acid in water were used as solvent systems. NMR spectra were recorded in CD₃OD, CDCl₃, or DMSO-*d*₆ either on a Bruker DRX 400 or Varian Unity Plus 300. Chemical shifts are reported as δ values from an internal tetramethylsilane standard. Mass spectral data were obtained on either a VG Bio-Q triple quadrupole mass spectrometer using electrospray ionization or a VG ZAB 2-SEQ mass spectrometer using FAB ionization. Accurate mass measurements were conducted with a Bruker Apex III FTICR mass spectrometer. Purity and characterization of compounds were established by a combination of LC-MS, high-resolution mass spectrometry (HRMS), and NMR analytical techniques. All compounds were found to be >95% pure by LC-MS and HRMS analysis.

1-Isopropylpiperidin-4-ylamine (5). (i) **(1-Isopropylpiperidin-4-yl)carbamic Acid *tert*-Butyl Ester.** To a solution

of piperidin-4-yl-carbamic acid *tert*-butyl ester (**4**) (5.0 g, 25 mmol) in 15 mL of methanol (15 mL) were added acetone (8 mL), Na(CN)BH₃ (3.14 g, 50 mmol), and acetic acid (0.3 mL). After the mixture was stirred for 16 h at room temperature, the solvent was removed under reduced pressure and the residue was partitioned between water (30 mL) and ethyl acetate (30 mL). The organic layer was washed with saturated Na₂CO₃ solution and water and then dried over Na₂SO₄. The solvent was removed under reduced pressure to give 4.8 g (80%) of product as a white solid. MS (ES) *m/z*: 243.4 (MH⁺).

(ii) **1-Isopropylpiperidin-4-ylamine (5).** To a solution of (1-isopropylpiperidin-4-yl)carbamic acid *tert*-butyl ester (4.8 g, 20 mmol) in methanol (15 mL) was added methanolic hydrochloric acid (8 M, 20 mL), and the mixture was stirred for 16 h. Removal of the solvent under reduced pressure, followed by removal of residual volatiles by twice coevaporating with toluene, gave 4.4 g (100%) of product **5**. ¹H NMR (DMSO-*d*₆): δ 8.52 (s, br., 2H), 3.36 (d, $J = 6.5$ Hz, 3H), 3.03 (d, $J = 11$ Hz, 2H), 2.51 (s, 1H), 2.15–2.01 (m, 4H), 1.26 (d, $J = 6.5$ Hz, 6H). MS (ES) *m/z*: 143.2 (MH⁺).

Ethyl 4-(5-Chlorothiophen-2-yl)-2,4-dioxobutanoate (7). Potassium *tert*-butoxide (17.5 g, 156 mmol) was added to a solution of 2-acetyl-5-chlorothiophene (**6**) (25 g, 156 mmol) in anhydrous toluene (400 mL) at 0 °C under nitrogen in four portions. The mixture was stirred at 0 °C for 10 min. Then diethyl oxalate (25 mL, 187 mmol) was added via syringe, and the resulting mixture was stirred at room temperature for 3 h. The precipitated product was collected by filtration, washed with toluene, and then dissolved in ethyl acetate (500 mL). The organic layer was washed with diluted aqueous hydrochloric acid (100 mL) and then dried over Na₂SO₄. Removal of the solvents afforded the desired product **7** as a yellow solid (25 g, 62%), which was used in the following reaction without further purification. ¹H NMR (CD₃OD): δ 7.87 (m, 1H), 7.15 (m, 1H), 6.95 (s, 1H), 4.35 (q, 2H, $J = 7.1$ Hz), 1.36 (t, 3H, $J = 7.1$ Hz). MS (ES) *m/z*: 261.0 (MH⁺).

Ethyl 5-(5-Chlorothiophen-2-yl)isoxazole-3-carboxylate (8). A mixture of ethyl 4-(5-chlorothiophen-2-yl)-2,4-dioxobutanoate (**7**) (25 g, 96 mmol) and hydroxylamine hydrochloride (25 g, 360 mmol) in anhydrous ethanol (300 mL) was refluxed for 5 h. The solvents were removed under reduced pressure, H₂O (150 mL) was added to the residue, followed by ammonium hydroxide (28–30%) to give pH 7. The aqueous mixture was then extracted with ethyl acetate (3 \times 100 mL), and the combined organic portions were dried over MgSO₄. After the solvents were removed, the crystalline product **8** (22 g, 89%) was used in the following reaction without further purification. ¹H NMR (CDCl₃): δ 7.31 (d, 1H, $J = 4.0$ Hz), 6.95 (d, 1H, $J = 4.0$ Hz), 6.71 (s, 1H), 4.44 (q, 2H, $J = 7.1$ Hz), 1.41 (t, 3H, $J = 7.1$ Hz). MS (ES) *m/z*: 258.0 (MH⁺).

(5-(5-Chlorothiophen-2-yl)isoxazol-3-yl)methanol. Sodium borohydride (16.1 g, 84.4 mmol) was added cautiously to the solution of ethyl 5-(5-chlorothiophen-2-yl)isoxazole-3-carboxylate (**8**) (22 g, 85 mmol) in anhydrous ethanol (250 mL) at 0 °C. The mixture was stirred at room temperature for 12 h. Ethanol was removed under reduced pressure, the residue was taken up in H₂O (100 mL), and dilute aqueous hydrochloric acid was added to give pH 3–4. The precipitated product was collected by filtration, washed with water, and dried in vacuo to give a pale-yellow solid (16 g, 67%). ¹H NMR (CDCl₃): δ 7.27 (d, 1H, $J = 3.9$ Hz), 6.94 (d, 1H, $J = 3.9$ Hz), 6.40 (s, 1H), 4.78 (s, 2H). MS (ES) *m/z*: 216.3 (MH⁺).

3-(Bromomethyl)-5-(5-chlorothiophen-2-yl)isoxazole (9). *N*-Bromosuccinimide (14.5 g, 82 mmol) was added to a mixture of (5-(5-chlorothiophen-2-yl)isoxazol-3-yl)methanol (3.50 g, 16.2 mmol) and polystyrene bound triphenyl phosphine (27 g, 81 mmol) in anhydrous methylene chloride (250 mL) at 0 °C. The mixture was stirred at room temperature for 1 h. The reaction mixture was filtered, and the filtrate was concentrated in vacuo. The residue was purified by flash column chromatography (10% of ethyl acetate/heptane) to yield 16.1 g (77%) of the product **9** as a white solid. ¹H NMR (CDCl₃): δ 4.42 (s, 2H), 6.42 (s, 1H), 6.95 (d, 1H, $J = 4.0$ Hz), 7.28 (d, 1H, $J = 4.0$

(Hz), 6.95 (d, 1H, $J = 4.0$ Hz), 6.42 (s, 1H), 4.42 (s, 2H). MS (ES) m/z : 279.1 (MH⁺).

Preparation of 1-[5-(5-Chlorothiophen-2-yl)isoxazol-3-ylmethyl]-6-methyl-1H-indole-2-carboxylic Acid (1-Isopropylpiperidin-4-yl)amide (13) (Scheme 2). (i) **6-Methyl-1H-indole-2-carboxylic Acid (11).** 2-Chloro-5-methylaniline (10) (2 g, 14.1 mmol), 2-oxopropionic acid (3.7 g, 42.4 mmol), acetic acid (1.2 mL, 21.2 mmol), and MgSO₄ (0.85 g, 7.1 mmol) were suspended in dimethylacetamide (100 mL). The tube was sealed with a serum cap, and argon was bubbled through the solution for 10 min. K₃PO₄ (3.9 g, 18.4 mmol) and Pd(*t*-Bu₃P)₂ (715 mg, 1.4 mmol) were added to the solution, and argon was bubbled through the mixture for an additional 10 min. The reaction mixture was heated to 140 °C in a preheated oil bath for 24 h. After cooling to room temperature, the reaction mixture was filtered, dichloromethane (150 mL) was added, and the mixture was extracted twice with 2 M NaOH (2 × 150 mL). The combined aqueous layers were acidified to pH 2 with 2 M hydrochloric acid and extracted with dichloromethane (3 × 150 mL). The combined organic layers were dried over MgSO₄ and filtered. After removal of the solvents under reduced pressure, the crude product **11** (1.1 g, 44%) was used without further purification for the next reaction step. ¹H NMR (DMSO-*d*₆): δ 12.75 (s, 1H), 8.53 (d, $J = 7.6$ Hz, 1H), 7.50 (d, 1H, $J = 7.9$ Hz, 1H), 7.21 (s, 1H), 7.02 (s, 1H), 6.90 (d, $J = 7.7$ Hz, 1H), 2.50 (s, 3H). MS (ES) m/z : 173.9 (M - H).

(ii) **6-Methyl-1H-indole-2-carboxylic Acid (1-Isopropylpiperidin-4-yl)amide (12).** To a solution of 6-methyl-1H-indole-2-carboxylic acid (**11**) (250 mg, 1.4 mmol) and *N*-ethylmorpholine (726 μL, 5.7 mmol) in dichloromethane (8 mL) was added *O*-(cyano(ethoxycarbonyl)methylene)amino-*N,N,N',N'*-tetramethyluronium tetrafluoroborate (TOTU) (468 mg, 1.4 mmol), and the mixture was stirred for 30 min at room temperature. **5** (304 mg, 1.4 mmol) was added, and the reaction was stirred for 16 h. After removal of the solvent under reduced pressure, the residue was purified by preparative reversed-phase HPLC, eluting with a gradient of acetonitrile in water (+0.01% trifluoroacetic acid). The product **12** was obtained in 250 mg (59%) yield as its trifluoroacetate salt. ¹H NMR (DMSO-*d*₆): δ 11.46 (s, 1H), 8.53 (d, $J = 7.6$ Hz, 1H), 7.48 (d, 1H, $J = 7.9$ Hz, 1H), 7.20 (s, 1H), 7.16 (s, 1H), 6.87 (d, $J = 7.7$ Hz, 1H), 6.57 (s, 1H), 4.09 (m, 1H), 3.43 (m, 2H), 3.14 (m, 2H), 2.50 (s, 3H), 2.09 (m, 2H), 2.02 (m, 1H), 1.80 (m, 2H), 1.25 (d, $J = 6.5$ Hz, 6H). MS (ES) m/z : 300.2 (MH⁺).

(iii) **1-[5-(5-Chlorothiophen-2-yl)isoxazol-3-ylmethyl]-6-methyl-1H-indole-2-carboxylic Acid (1-Isopropylpiperidin-4-yl)amide (13).** 6-Methyl-1H-indole-2-carboxylic acid (1-isopropylpiperidin-4-yl)amide (**12**) (222 mg; 0.8 mmol) was dissolved in DMF (2 mL), and sodium hydride (60% in oil, 31 mg, 0.8 mmol) was added. The solution was stirred at room temperature for 20 min, then **9** (214 mg, 0.8 mmol) was added and the reaction mixture was heated to 80 °C for 16 h. After the mixture was cooled to room temperature, saturated NaHCO₃ solution (10 mL) was added, and the reaction mixture was extracted with ethyl acetate (3 × 50 mL). The combined organic layers were dried over MgSO₄ and filtered. After removal of the solvents under reduced pressure, the product was purified by preparative reversed-phase HPLC, eluting with a gradient of acetonitrile in water (+0.01% trifluoroacetic acid). Following lyophilization, the product **13** was obtained in 30 mg (15%) yield as its trifluoroacetate salt. ¹H NMR (DMSO-*d*₆): δ 8.58 (d, $J = 7.6$ Hz, 1H), 7.56 (m, 3H), 7.39 (s, 1H), 7.27 (d, 4.2 Hz, 1H), 7.00 (s, 1H), 6.98 (d, $J = 7.7$ Hz, 1H), 5.86 (s, 2H), 4.05 (m, 1H), 3.43 (m, 2H), 3.14 (m, 2H), 2.50 (s, 3H), 2.09 (m, 2H), 2.02 (m, 1H), 1.80 (m, 2H), 1.25 (d, $J = 6.5$ Hz, 6H). MS (ES) m/z : 497.2 (MH⁺). HRMS calcd for C₂₆H₃₀ClN₄O₂S 497.1773; found 497.1769.

1-[5-(5-Chlorothiophen-2-yl)isoxazol-3-ylmethyl]-3-methyl-1H-indole-2-carboxylic Acid (1-Isopropylpiperidin-4-yl)amide (17) (Scheme 2). (i) **3-Methyl-1H-indole-2-carboxylic Acid (15).** 2-Iodophenylamine (**14**) (0.9 g, 4 mmol), 2-oxobutanoic acid (1.2 g, 12 mmol), 1,4-diazabicyclo[2.2.2]octane (1.3 g, 12 mmol), and MgSO₄ (0.85 g, 7.1 mmol) were suspended in DMF (12 mL). The round-bottom flask was

sealed with a serum cap, and argon was bubbled through the solution for 10 min. Pd(OAc)₂ (93 mg, 0.2 mmol) was added to the solution, and argon was bubbled through the mixture for an additional 10 min. The reaction mixture was heated to the 105 °C for 16 h. After cooling to room temperature, the reaction mixture was filtered, dichloromethane (150 mL) was added, and the mixture was extracted twice with 2 M NaOH (2 × 150 mL). The combined aqueous layers were acidified to pH 2 with 2 M hydrochloric acid and extracted with dichloromethane (3 × 150 mL). The combined organic layers were dried over MgSO₄ and filtered. After removal of the solvents under reduced pressure, the crude product **15** (770 mg, 55%) was used without further purification for the next reaction step. ¹H NMR (CDCl₃): δ 7.62 (d, $J = 8.2$ Hz, 1H), 7.38 (d, $J = 7.9$ Hz, 1H), 7.18 (dd, $J = 8.0$ Hz, $J = 7.0$ Hz, 1H), 7.05 (dd, $J = 8.0$ Hz, $J = 7.0$ Hz, 1H), 2.48 (s, 3H). MS (ES) m/z : 176.1 (MH⁺).

(ii) ***N*-(1-Isopropylpiperidin-4-yl)-3-methyl-1H-indole-2-carboxamide (16).** To a solution of 3-methyl-1H-indole-2-carboxylic acid (**15**) (300 mg 1.72 mmol) in dichloromethane (10 mL) and NEt₃ (1 mL, 6.8 mmol) was added bis(oxo-3-oxazolidinyl)phosphoryl chloride (BOP-Cl) (435 mg, 1.72 mmol) at room temperature, and the mixture was stirred for 5 min. After addition of **5** (487 mg 2.2 mmol), the mixture was stirred for 16 h. The reaction mixture was diluted with dichloromethane (100 mL) and washed with brine (50 mL). The organic layer was dried over MgSO₄ and filtered. After removal of the solvents under reduced pressure, the crude product **16** (506 mg, 99%) was used without further purification for the next reaction step. ¹H NMR (CDCl₃): δ 7.60 (d, $J = 8.0$ Hz, 1H), 7.36 (d, $J = 7.8$ Hz, 1H), 7.18 (dd, $J = 8.0$ Hz, $J = 7.0$ Hz, 1H), 7.02 (dd, $J = 8.1$ Hz, $J = 7.3$ Hz, 1H), 4.09 (m, 1H), 2.93 (m, 2H), 2.84 (m, 2H), 2.51 (s, 3H), 2.41 (m, 2H), 2.12 (m, 1H), 1.70 (m, 2H), 1.25 (d, $J = 6.5$ Hz, 6H). MS (ES) m/z : 300.4 (MH⁺).

(iii) **1-[5-(5-Chlorothiophen-2-yl)isoxazol-3-ylmethyl]-3-methyl-1H-indole-2-carboxylic Acid (1-Isopropylpiperidin-4-yl)amide (17).** *N*-(1-Isopropylpiperidin-4-yl)-3-methyl-1H-indole-2-carboxamide (**16**) (100 mg, 0.33 mmol) was dissolved in DMF (2 mL), and sodium hydride (60% in oil, 15 mg, 0.4 mmol) was added. The solution was stirred at room temperature for 20 min. Then **9** (107 mg, 0.4 mmol) was added, and the reaction mixture was heated to 70 °C for 5 h. Then, after the mixture was cooled to room temperature, a saturated NaHCO₃ solution (10 mL) was added. The reaction mixture was then extracted with ethyl acetate (3 × 50 mL). The combined organic layers were dried over MgSO₄ and filtered. After removal of the solvents under reduced pressure, the product was purified by preparative reversed-phase HPLC, eluting with a gradient of acetonitrile in water (+0.01% trifluoroacetic acid). Following lyophilization, the product **17** was obtained in 16 mg (10%) yield. ¹H NMR (DMSO-*d*₆): δ 8.56 (d, $J = 7.7$ Hz, 1H), 7.66–7.60 (m, 3H), 7.57–7.52 (m, 2H), 7.30 (ddd, $J = 8.0$ Hz, $J = 7.0$ Hz, $J = 1.0$ Hz, 1H), 7.27 (d, $J = 4.1$ Hz, 1H), 7.13 (dd, $J = 8.0$ Hz, $J = 7.0$ Hz, 1H), 6.59 (s, 1H), 5.64 (s, 2H), 4.11 (m, 1H), 3.43 (m, 2H), 3.13 (m, 2H), 2.38 (s, 3H), 2.07 (m, 2H), 2.02 (m, 1H), 1.82 (m, 2H), 1.26 (d, $J = 6.6$ Hz, 6H). MS (ES) m/z : 497.1 (MH⁺). HRMS calcd for C₂₆H₃₀ClN₄O₂S 497.1778; found 497.1776.

Preparation of 1-[5-(5-Chlorothiophen-2-yl)isoxazol-3-ylmethyl]-3-cyano-7-methyl-1H-indole-2-carboxylic Acid (1-Isopropylpiperidin-4-yl)amide (21) (Scheme 2). (i) **7-Methyl-1H-indole-2-carboxylic Acid Methyl Ester.** 7-Methyl-1H-indole-2-carboxylic acid (**18**) (1.0 g, 57 mmol) was dissolved in methanolic hydrochloric acid (8 M, 20 mL), and the mixture was stirred at room temperature for 16 h. After removal of the solvent under reduced pressure, residual volatiles were removed by codistillation twice with toluene (2 × 10 mL). The remaining slightly yellow solid (1.1 g, 100%) was subjected to the subsequent reaction without further purification. MS (ES) m/z : 190.4 (MH⁺).

(ii) **3-Iodo-7-methyl-1H-indole-2-carboxylic Acid Methyl Ester.** 7-Methyl-1H-indole-2-carboxylic acid methyl ester (1.08 g, 5.7 mmol) was dissolved in dichloromethane (15 mL),

and *N*-iodosuccinimide (1.41 g, 6.3 mmol) was added. The solution was stirred for 16 h at room temperature, then washed with aqueous sodium thiosulfate solution. The organic phase was dried (Na₂SO₄) and filtered through a silica gel cartridge, washing with dichloromethane. The solvent was removed under reduced pressure to give the product in 1.69 g (94%) yield. ¹H NMR (DMSO-*d*₆): δ 12.09 (s, 1H), 7.21 (d, *J* = 8.0 Hz, 1H), 7.12 (d, 1H, *J* = 7.3 Hz, 1H), 7.21 (m, 1H), 3.92 (s, 3H), 2.54 (s, 3H). MS (ES) *m/z*: 316 (MH⁺).

(iii) **3-Cyano-7-methyl-1*H*-indole-2-carboxylic Acid Methyl Ester (19)**. 3-Iodo-7-methyl-1*H*-indole-2-carboxylic acid methyl ester (1.69 g, 5.4 mmol), CuCN (0.96 g, 10.8 mmol), and tetraethylammonium cyanide (0.42 g, 2.7 mmol) were dissolved in DMF (15 mL) and THF (15 mL), and the mixture was purged with argon for 15 min. 1,1'-Bis(diphenylphosphino)ferrocene (0.45 g, 0.8 mmol) and Pd₂(dba)₃ (0.246 g, 0.3 mmol) were added. The reaction mixture was heated to 120 °C for 5 h, then the solvent was removed under reduced pressure. The residue was dissolved in ethyl acetate and washed with a saturated aqueous NaHCO₃ solution. The organic phase was dried (Na₂SO₄), filtered, and evaporated. The product was purified first by silica gel chromatography, eluting with a gradient of ethyl acetate in heptane, followed by preparative reversed-phase HPLC, eluting with a gradient of acetonitrile in water (+0.01% trifluoroacetic acid). The product **19** was obtained in 0.15 g (13%) yield. ¹H NMR (DMSO-*d*₆): δ 12.97 (s, 1H), 7.82 (d, *J* = 8.3 Hz, 1H), 7.46 (m, 1H), 7.25 (d, *J* = 8.4 Hz, 1H), 3.92 (s, 3H), 2.54 (s, 3H). MS (ES) *m/z*: 215 (MH⁺).

(iv) **1-[(5-(5-Chlorothiophen-2-yl)isoxazol-3-yl)methyl]-3-cyano-7-methyl-1*H*-indole-2-carboxylic Acid (20)**. 3-Cyano-7-methyl-1*H*-indole-2-carboxylic acid methyl ester (**19**) (150 mg, 0.7 mmol) was dissolved in DMF (2 mL), and sodium hydride (60% in oil, 31 mg, 0.8 mmol) was added. The solution was stirred at room temperature for 20 min, then cooled to -70 °C. **9** (214 mg, 0.8 mmol) was added, and the reaction mixture was allowed to warm to room temperature. The reaction mixture was stirred for 3 h. Then 2 M aqueous NaOH solution (0.5 mL) was added, and the reaction mixture was stirred for 16 h. The product was purified by preparative reversed-phase HPLC, eluting with a gradient of acetonitrile in water (+0.01% trifluoroacetic acid). Following lyophilization the product **20** was obtained in 113 mg (39%) yield. ¹H NMR (DMSO-*d*₆): δ 14.3 (s, 1H), 7.56 (m, 2H), 7.28 (m, 3H), 6.79 (s, 1H), 6.21 (s, 2H), 2.66 (s, 3H). MS (ES) *m/z*: 398 (MH⁺).

(v) **1-[5-(5-Chlorothiophen-2-yl)isoxazol-3-ylmethyl]-3-cyano-7-methyl-1*H*-indole-2-carboxylic Acid (1-Isopropylpiperidin-4-yl)amide (21)**. To a solution of 1-[(5-(5-chlorothiophen-2-yl)isoxazol-3-yl)methyl]-3-cyano-7-methyl-1*H*-indole-2-carboxylic acid (**20**) (30 mg, 75 μmol) and *N*-ethylmorpholine (38 μL) in dichloromethane (8 mL) was added *O*-((cyano(ethoxycarbonyl)methylene)amino)-*N,N,N,N*-tetramethyluronium tetrafluoroborate (TOTU) (25 mg, 75 μmol), and the mixture was stirred for 30 min at room temperature. Then **5** (32 mg, 0.15 mmol) was added, and the reaction mixture was stirred for 16 h. After removal of the solvent under reduced pressure, the residue was purified by preparative reversed-phase HPLC, eluting with a gradient of acetonitrile in water (+0.01% trifluoroacetic acid). The product **21** was obtained in 22 mg (46%) yield as its trifluoroacetate salt. ¹H NMR (DMSO-*d*₆): δ 9.37 (d, *J* = 7.7 Hz, 1H), 7.56 (m, 2H), 7.29 (d, *J* = 4.0 Hz, 1H), 7.26 (m, 2H), 7.20 (d, *J* = 8.4 Hz, 1H), 6.67 (s, 1H), 5.94 (s, 2H), 4.11 (m, 1H), 3.42 (m, 2H), 3.12 (m, 2H), 2.70 (s, 3H), 2.07 (m, 2H), 2.02 (m, 1H), 1.84 (m, 2H), 1.26 (d, *J* = 6.5 Hz, 6H). MS (ES) *m/z*: 522.2 (MH⁺). HRMS calcd for C₂₇H₂₉ClN₅O₂S 522.1730; found 522.1725.

Representative Procedure: Preparation of 1-[5-(5-Chlorothiophen-2-yl)isoxazol-3-ylmethyl]-1*H*-indole-2-carboxylic Acid (1-Isopropylpiperidin-4-yl)amide (1). (i) **1*H*-Indole-2-carboxylic Acid Methyl Ester**. 1*H*-Indole-2-carboxylic acid (2.0 g, 124 mmol) was dissolved in methanolic hydrochloric acid (8 M, 30 mL), and the mixture was stirred at room temperature for 16 h. After removal of the solvent under reduced pressure, residual volatiles were removed by

codistillation with toluene (2 × 10 mL). The remaining slightly yellow solid (2.3 g, 100%) was subjected to the subsequent reaction without further purification. MS (ES) *m/z*: 176.6 (MH⁺).

(ii) **1-[5-(5-Chlorothiophen-2-yl)isoxazol-3-ylmethyl]-1*H*-indole-2-carboxylic Acid Methyl Ester**. To a solution of 1*H*-indole-2-carboxylic acid methyl ester (244.2 mg, 1.4 mmol) in DMF (2 mL) was added sodium hydride (60% in oil, 52.2 mg, 1.3 mmol) at room temperature. After the mixture was stirred for 30 min, **9** (500 mg, 1.8 mmol) was added and the mixture was heated for 1 h at 80 °C. After cooling of the reaction mixture to room temperature and addition of water (5 mL), the mixture was filtered through a pad of Celite, washing with ethyl acetate. After concentration under reduced pressure the product (288 mg, 55%) was directly subjected to the subsequent saponification reaction without further purification. MS (ES) *m/z*: 373.6 (MH⁺).

(iii) **1-[5-(5-Chlorothiophen-2-yl)isoxazol-3-ylmethyl]-1*H*-indole-2-carboxylic Acid**. To a solution of 1-[5-(5-chlorothiophen-2-yl)isoxazol-3-ylmethyl]-1*H*-indole-2-carboxylic acid methyl ester (288 mg, 0.77 mmol) in THF (10 mL) were added water (3 mL) and lithium hydroxide monohydrate (57.0 mg, 1.4 mmol). After the mixture was stirred for 2 h at 60 °C, the reaction mixture was cooled to room temperature. The mixture was acidified to pH 3 with half-concentrated hydrochloric acid. The resulting precipitate was collected by filtration and washed with water (3 mL). The product (253 mg, 92%) was obtained as a white solid, which was dried under reduced pressure. MS (ES) *m/z*: 359.4 (MH⁺).

(iv) **1-[5-(5-Chlorothiophen-2-yl)isoxazol-3-ylmethyl]-1*H*-indole-2-carboxylic Acid (1-Isopropylpiperidin-4-yl)amide (1)**. To a solution of 1-[5-(5-chlorothiophen-2-yl)isoxazol-3-ylmethyl]-1*H*-indole-2-carboxylic acid (117 mg, 0.33 mmol) in dichloromethane (1 mL) were added NEt₃ (0.17 mL, 1.2 mmol) and bis(oxo-3-oxazolidinyl)phosphoryl chloride (BOP-Cl) (79 mg, 0.33 mmol) at room temperature, and the mixture was stirred for 30 min. After addition of **5** (81 mg, 0.37 mmol), the mixture was stirred for 16 h. After removal of the solvent under reduced pressure, the residue was purified by preparative HPLC (C18 reverse phase column, eluting with a gradient of acetonitrile in water (+0.01% trifluoroacetic acid). The fractions containing the product were evaporated and lyophilized to yield the product **1** (93 mg, 60%) as a white solid. The product was obtained as its trifluoroacetate salt. ¹H NMR (DMSO-*d*₆): δ 8.65 (d, *J* = 7.5 Hz, 1H), 7.69 (d, *J* = 8.0 Hz, 1H), 7.60 (d, *J* = 8.0 Hz, 1H), 7.54 (d, *J* = 4.0 Hz, 1H), 7.30 (ddd, *J* = 8.0 Hz, *J* = 7.0 Hz, *J* = 1.0 Hz, 1H), 7.26 (d, *J* = 4.0 Hz, 1H), 7.23 (s, 1H), 7.15 (ddd, *J* = 8.0 Hz, *J* = 7.0 Hz, *J* = 1.0 Hz, 1H), 6.58 (s, 1H), 5.91 (s, 2H), 4.06 (m, 1H), 3.43 (m, 2H), 3.10 (m, 2H), 2.07 (m, 2H), 2.02 (m, 1H), 1.80 (m, 2H), 1.26 (d, *J* = 6.5 Hz, 6H). MS (ES) *m/z*: 483.3 (MH⁺). HRMS calcd for C₂₅H₂₈ClN₄O₂S 483.1621; found 483.1616.

1-[5-(5-Chlorothiophen-2-yl)isoxazol-3-ylmethyl]-3-fluoro-1*H*-indole-2-carboxylic Acid (1-Isopropylpiperidin-4-yl)amide (22). To a solution of **1** (40 mg, 0.08 mmol) in dichloromethane (1 mL) was added *N*-fluoropyridinium triflate (22 mg, 0.09 mmol), and the mixture was stirred at room temperature for 4 days. The reaction mixture was directly purified by preparative reversed-phase HPLC, eluting with a gradient of acetonitrile in water (+0.01% trifluoroacetic acid). After lyophilization the product **22** (22 mg, 50%) was obtained as white solid. ¹H NMR (DMSO-*d*₆): δ 8.59 (d, *J* = 7.8 Hz, 1H), 7.75 (dd, *J* = 8.1 Hz, *J* = 7.0 Hz, 1H), 7.54 (d, *J* = 4.0 Hz, 1H), 7.41 (ddd, *J* = 8.0 Hz, *J* = 7.0 Hz, *J* = 1.0 Hz, 1H), 7.28 (m, 3H), 6.60 (s, 1H), 5.76 (s, 2H), 4.08 (m, 1H), 3.43 (m, 2H), 3.10 (m, 2H), 2.07 (m, 2H), 2.02 (m, 1H), 1.82 (m, 2H), 1.26 (d, *J* = 6.5 Hz, 6H). MS (ES) *m/z*: 501.2 (MH⁺). HRMS calcd for C₂₅H₂₇ClFN₄O₂S 501.1527; found 501.1522.

3-Chloro-1-[5-(5-chlorothiophen-2-yl)isoxazol-3-ylmethyl]-1*H*-indole-2-carboxylic Acid (1-Isopropylpiperidin-4-yl)amide (23). To a solution of **1** (40 mg, 0.08 mmol) in dichloromethane (1 mL) was added *N*-chlorosuccinimide (17 mg, 0.13 mmol), and the mixture was stirred at room temperature for 16 h. The reaction mixture was directly purified by

preparative reversed-phase HPLC, eluting with a gradient of acetonitrile in water (+0.01% trifluoroacetic acid). After lyophilization the product **23** (15 mg, 36%) was obtained as a white solid. ¹H NMR (DMSO-*d*₆): δ 8.81 (d, *J* = 7.8 Hz, 1H), 7.75 (d, *J* = 8.5 Hz, 1H), 7.60 (d, *J* = 7.5 Hz, 1H), 7.57 (d, *J* = 7.7 Hz, 1H), 7.55 (d, *J* = 4.0 Hz, 1H), 7.41 (ddd, *J* = 8.0 Hz, *J* = 7.0 Hz, *J* = 1.0 Hz, 1H), 7.28 (d, *J* = 4.1 Hz, 1H), 6.62 (s, 1H), 5.70 (s, 2H), 4.06 (m, 1H), 3.43 (m, 2H), 3.10 (m, 2H), 2.07 (m, 2H), 2.02 (m, 1H), 1.82 (m, 2H), 1.26 (d, *J* = 6.6 Hz, 6H). MS (ES) *m/z*: 517.2 (MH⁺). HRMS calcd for C₂₅H₂₇Cl₂N₄O₂S 517.1231; found 517.1226.

3-Bromo-1-[5-(5-chlorothiophen-2-yl)isoxazol-3-yl-methyl]-1H-indole-2-carboxylic Acid (1-Isopropylpiperidin-4-yl)amide (24). To a solution of **1** (40 mg, 0.08 mmol) in dichloromethane (1 mL) was added *N*-bromosuccinimide (176 mg, 0.13 mmol), and the mixture was stirred at room temperature for 16 h. The reaction mixture was directly purified by preparative reversed-phase HPLC, eluting with a gradient of acetonitrile in water (+0.01% trifluoroacetic acid). After lyophilization the product **24** (18 mg, 40%) was obtained as a white solid. ¹H NMR (DMSO-*d*₆): δ 8.82 (d, *J* = 7.8 Hz, 1H), 7.72 (d, *J* = 8.5 Hz, 1H), 7.57–7.52 (m, 3H), 7.41 (ddd, *J* = 8.0 Hz, *J* = 7.0 Hz, *J* = 1.0 Hz, 1H), 7.27 (d, *J* = 4.1 Hz, 1H), 6.52 (s, 1H), 5.99 (s, 2H), 4.06 (m, 1H), 3.43 (m, 2H), 3.10 (m, 2H), 2.07 (m, 2H), 2.02 (m, 1H), 1.82 (m, 2H), 1.26 (d, *J* = 6.6 Hz, 6H). MS (ES) *m/z*: 561.1 (MH⁺). HRMS calcd for C₂₅H₂₇BrClN₄O₂S 561.0726; found 561.0721.

5.2. X-ray Structure Analysis. Crystallization. Purified human fXa was purchased from Enzyme Research Lab (South Bend, IN). The Gla-domain was removed, and the Gla-less factor Xa was crystallized in hanging drops as described earlier.¹⁸

Data Collection and Processing. Crystals were soaked in 5 μL of reservoir solution containing ~20 mM saturated inhibitor (depending on the solubility) for 24–72 h. Data were collected at cryotemperatures. The crystals were picked up with a fiber loop, soaked for a few seconds in a solution containing 20% glycerol and 5–20 mM inhibitor in reservoir solution, and flash-frozen in a stream of gaseous nitrogen at 100 K.

The X-ray intensity data were collected on a 130 mm Mar CCD detector mounted on an Elliot GX-13 “big wheel” rotating anode generator (Nonius, The Netherlands), operating at 40 kV and 55 mA, or on a Mar300 imaging plate (X-ray research, Germany) mounted on an FR591 rotating anode (Nonius, The Netherlands), operating at 40 kV and 80 mA. Data processing and scaling were carried out using the XDS package.²⁰ Data collection and refinement statistics for selected crystal structures are presented in Table 4.

Structure Solution and Crystallographic Refinement.

The structures were solved by molecular replacement. The search models were made from the coordinates of refined structures of fXa complexes solved previously with the same crystal packing as the current complexes. The bound inhibitors were omitted from the search models. Energy-restrained least-squares refinement was carried out using X-PLOR.²¹ This refinement was started with rigid body refinement to adjust for small differences in cell dimensions, followed by energy minimization and individual temperature factor refinement. At this stage the $2F_o - F_c$ and $F_o - F_c$ maps were inspected and the inhibitors were fitted. Solvent molecules were included if they were on sites of difference electron density with values above 3.5σ and if they were within 3.5 Å of the protein molecule or a water molecule. After two to three additional rounds of manual inspection, rebuilding, and refinement, final models were obtained with *R*-factors between 18.1% and 21.8% and free *R*-factors between 25.3% and 29.8% plus good geometry. The EGF-1 domain is not visible in the electron density maps probably because of disorder, and the rather high free *R*-factors might relate to this disordered EGF-1 domain. The statistics of the crystallographic refinement are listed in Table 4.

3. Computational procedures. Docking Studies. Factor Xa crystal structures were taken from RSCB²² and from our

internal database and were used for flexible docking studies. After analysis of protein–ligand interactions using the program GRID,²³ molecules were manually oriented and minimized within the binding site or automatically docked into the active site using the program QXP²⁴ employing a modified version of the AMBER force field.²⁵ Selected protein side chains were treated as flexible for minimization and Monte Carlo searching after comparative analysis of fXa X-ray structures. Selected conformers are subsequently optimized using the MMFF94s force field²⁶ implemented in Sybyl.²⁷ Protein/ligand complexes were minimized using quasi-Newton–Raphson (BFGS) or conjugate gradient (CG) procedures with all protein atoms as rigid. The program MOLCAD²⁸ was used to visualize properties such as lipophilicity^{29,30} and cavity depth on solvent-accessible protein surfaces.³¹

Acknowledgment. We thank A. Sihorsch, M. Kämmerer-Dienst, L. Bayer, N. Laub, D. Timme, F. Gerstmann, A. Liesum, V. Brachvogel, P. Loenze, and S. Engel for their excellent technical assistance.

Supporting Information Available: Experimental data for the compounds **25–46** and purity data of all compounds. This material is available free of charge via the Internet at <http://pubs.acs.org>. The coordinates of the fXa complexes were deposited in the Brookhaven Protein Data Bank (accession codes 2BOH, 2BQ6, 2BQ7, 2BQW, 1LQD).

References

- (1) Vlasuk, G. P. Direct Factor Xa inhibitors. In *New Therapeutic Agents in Thrombosis and Thrombolysis*; Sasahara, A. A., Loscalzo, J., Eds.; Marcel Dekker: New York, 1997; pp 261–283.
- (2) (a) Hirsh, J. Heparin. *N. Engl. J. Med.* **1991**, *324*, 1565–1574. (b) Freedman, M. D. Warfarin and other “anti-vitamin K anticoagulants. Pharmacodynamics and clinical use. *Am J. Ther.* **1996**, *3*, 771–783. (c) Raj, G.; Kumar, R.; McKinney, W. P. Long-term oral anticoagulant therapy: update on indications, therapeutic ranges, and monitoring. *Am. J. Med. Sci.* **1994**, *307*, 128–32.
- (3) (a) Coleman, R. W., Marder, V. J., Salzman, E. W., Eds. *Hemostasis and Thrombosis: Basic Principles and Clinical Practice*; J. B. Lippincott: Philadelphia, PA, 1994. (b) Davie, E. W.; Fujikawa, K.; Kisiel, W. The coagulation cascade: initiation, maintenance, and regulation. *Biochemistry* **1991**, *30*, 10363–10370. (c) Leadley, R. J. Coagulation factor Xa inhibition: biological background and rationale. *Curr. Top. Med. Chem.* **2001**, *1*, 151–159. (d) Stassen, J. M.; Arnout, J.; Deckmyn, H. The hemostatic system. *Curr. Med. Chem.* **2004**, *11*, 2245–2260.
- (4) Kaiser, B. Thrombin and factor Xa inhibitors. *Drugs Future* **1998**, *23*, 423–436.
- (5) (a) Pinto, D. J. P.; Orwat, M. J.; Wang, S.; Fevig, J. M.; Quan, M. L.; Amparo, E.; Cacciola, J.; Rossi, K. A.; Alexander, R. S.; Smallwood, A. M.; Luettgen, J. M.; Liang, L.; Aungst, B. J.; Wright, M. R.; Knabb, R. M.; Wong, P. C.; Wexler, R. R.; Lam, P. Y. S. Discovery of 1-[3-(Aminomethyl)phenyl]-*N*-[3-fluoro-2-(methylsulfonyl)-[1,1'-biphenyl]-4-yl]-3-(trifluoromethyl)-1*H*-pyrazole-5-carboxamide (DPC423), a highly potent, selective, and orally bioavailable inhibitor of blood coagulation factor Xa. *J. Med. Chem.* **2001**, *44*, 566–578. (b) Pauls, H. W.; Ewing, W. R. The design of competitive, small-molecule inhibitors of coagulation Factor Xa. *Curr. Top. Med. Chem.* **2001**, *1*, 83–100.
- (6) (a) Song, Y.; Clizbe, L.; Bhakta, C.; Teng, W.; Wong, P.; Huang, B.; Tran, K.; Sinha, U.; Park, G.; Reed, A.; Scarborough, R. M.; Zhu, B.-Y. Design and synthesis of factor Xa inhibitors and their prodrugs. *Bioorg. Med. Chem. Lett.* **2003**, *13*, 297–300. (b) Gustafsson, D.; Elg, M. The pharmacodynamics and pharmacokinetics of the oral direct thrombin inhibitor Ximelagatran and its active metabolite Melagatran: a mini-review. *Thromb. Res.* **2003**, *109* (Suppl. 1), S9–S15. (c) Koshio, H.; Hirayama, F.; Ishihara, T.; Kaizawa, H.; Shigenaga, T.; Taniuchi, Y.; Sato, K.; Moritani, Y.; Iwatsuki, Y.; Uemura, T.; Kaku, S.; Kawasaki, T.; Matsumoto, Y.; Sakamoto, S.; Tsukamoto, S.-I. Orally active factor Xa inhibitor: synthesis and biological activity of masked amidines as prodrugs of novel 1,4-diazepane derivatives. *Bioorg. Med. Chem.* **2004**, *12*, 5415–5426.
- (7) (a) Quan, M. L.; Lam, P. Y. S.; Han, Q.; Pinto, D. J. P.; He, M. Y.; Li, R.; Ellis, C. D.; Clark, C. G.; Teleha, C. A.; Sun, J.-H.; Alexander, R. S.; Bai, S.; Luettgen, J. M.; Knabb, R. M.; Wong, P. C.; Wexler, R. R. Discovery of 1-(3'-aminobenzisoxazol-5'-yl)-3-trifluoromethyl-*N*-[2-fluoro-4-[(2'-dimethylaminomethyl)imidazol-1-yl]phenyl]-1*H*-pyrazole-5-carboxamide hydrochloride (raza-

- xaban), a highly potent, selective, and orally bioavailable factor Xa inhibitor. *J. Med. Chem.* **2005**, *48*, 1729–1744. (b) Lam, P. Y. S.; Clark, C. G.; Li, R.; Pinto, D. J. P.; Orwat, M. J.; Galemno, R. A.; Fevig, J. M.; Teleha, C. A.; Alexander, R. S.; Smallwood, A. M.; Rossi, K. A.; Wright, M. R.; Bai, S. A.; He, K.; Luettgen, J. M.; Wong, P. C.; Knabb, R. M.; Wexler, R. R. Structure-based design of novel guanidine/benzamidine mimics: potent and orally bioavailable factor Xa inhibitors as novel anticoagulants. *J. Med. Chem.* **2003**, *46*, 4405–4418.
- (8) (a) Adler, M.; Kochanny, M. J.; Ye, B.; Rummenik, G.; Light, D. R.; Biancalana, S.; Whitlow, M. Crystal structures of two potent nonamidine inhibitors bound to factor Xa. *Biochemistry* **2002**, *41*, 15514–15523. (b) Maignan, S.; Guilloteau, J.-P.; Choi-Sledeski, Y. M.; Becker, M. R.; Ewing, W. R.; Pauls, H. W.; Spada, A. P.; Mikol, V. Molecular structures of human factor Xa complexed with ketopiperazine inhibitors: Preference for a neutral group in the S1 pocket. *J. Med. Chem.* **2003**, *46*, 685–690.
- (9) (a) Nazaré, M.; Essrich, M.; Will, D. W.; Matter, H.; Ritter, K.; Urmann, M.; Bauer, A.; Schreuder, H.; Czech, J.; Lorenz, M.; Laux, V.; Wehner, V. Novel factor Xa inhibitors based on a 2-carboxyindole scaffold: SAR of P4 substituents in combination with a neutral P1 ligand. *Bioorg. Med. Chem. Lett.* **2004**, *14*, 4197–4201. (b) Nazaré, M.; Essrich, M.; Will, D. W.; Matter, H.; Ritter, K.; Urmann, M.; Bauer, A.; Schreuder, H.; Dudda, A.; Czech, J.; Lorenz, M.; Laux, V.; Wehner, V. Factor Xa inhibitors based on a 2-carboxyindole scaffold: SAR of neutral P1 substituents. *Bioorg. Med. Chem. Lett.* **2004**, *14*, 4191–4195.
- (10) (a) Fevig, J. M.; Wexler, R. R. Anticoagulants: thrombin and factor Xa inhibitors. *Annu. Rep. Med. Chem.* **1999**, *34*, 81–100. (b) Zhu, B.-Y.; Scarborough, R. M. Recent advances in inhibitors of factor Xa in the prothrombinase complex. *Curr. Opin. Cardiovasc., Pulm. Renal Invest. Drugs* **1999**, *1*, 63–87. (c) Ewing, W. R.; Pauls, H. W.; Spada, A. P. Progress in the design of inhibitors of coagulation factor Xa. *Drugs Future* **1999**, *24*, 771–787. (d) Zhu, B.-Y.; Scarborough, R. M. Factor Xa inhibitors: recent advances in anticoagulant agents. *Annu. Rep. Med. Chem.* **2000**, *35*, 83–102. (e) Sanderson, P. E. J. Anticoagulants: Inhibitors of thrombin and factor Xa. *Annu. Rep. Med. Chem.* **2001**, *36*, 79–88. (f) Walenga, J. M.; Jeske, W. P.; Hoppensteadt, D.; Fareed, J. Factor Xa inhibitors: Today and beyond. *Curr. Opin. Invest. Drugs* **2003**, *4*, 272–281. (g) Ries, U. J.; Pripke, H. W. M. Factor Xa inhibitors—a review of the recent patent literature. *IDrugs* **2000**, *3*, 1509–1524.
- (11) Choi-Sledeski, Y. M.; Kearney, R.; Poli, G.; Pauls, H.; Gardner, C.; Gong, Y.; Becker, M.; Davis, R.; Spada, A.; Liang, G.; Chu, V.; Brown, K.; Collussi, D.; Leadley, R., Jr.; Rebello, S.; Moxey, P.; Morgan, S.; Bentley, R.; Kasiewski, C.; Maignan, S.; Guilloteau, J.-P.; Mikol, V. Discovery of an orally efficacious inhibitor of coagulation factor Xa which incorporates a neutral P1 ligand. *J. Med. Chem.* **2003**, *46*, 681–684.
- (12) Jia, Z. J.; Wu, Y.; Huang, W.; Zhang, P.; Clizbe, L. A.; Goldman, E. A.; Sinha, U.; Arfsten, A. E.; Edwards, S. T.; Alphonso, M.; Hutchaleelaha, A.; Scarborough, R. M.; Zhu, B.-Y. 1-(2-Naphthyl)-1H-pyrazole-5-carboxylamides as potent factor Xa inhibitors. Part 2: A survey of P4 motifs. *Bioorg. Med. Chem. Lett.* **2004**, *14*, 1221–1227.
- (13) Nazaré, M.; Matter, H.; Klingler, O.; Al-Obeidi, F.; Schreuder, H.; Zoller, G.; Czech, J.; Lorenz, M.; Dudda, A.; Peyman, A.; Nestler, H. P.; Urmann, M.; Bauer, A.; Laux, V.; Wehner, V.; Will, D. W. Novel factor Xa inhibitors based on a benzoic acid scaffold and incorporating a neutral P1 ligand. *Bioorg. Med. Chem. Lett.* **2004**, *14*, 2801–2805.
- (14) Matter, H.; Will, D. W.; Nazaré, M.; Schreuder, H.; Laux, V.; Wehner, V. Structural requirements for factor Xa inhibition by 3-oxylbenzamides with neutral P1 substituents: Combining X-ray crystallography, 3D-QSAR and tailored scoring functions. *J. Med. Chem.* **2005**, *48*, 3290–3312.
- (15) In vitro assays for determination of fXa activity were performed as described in the following: Ostrem, J. A.; Al-Obeidi, F. A.; Safar, P.; Safarova, A.; Stringer, S. K.; Patek, M.; Cross, M. T.; Spoonamore, J.; LoCascio, J. C.; Kasireddy, P.; Thorpe, D.; Sepetov, N.; Lebl, M.; Wildgoose, P.; Strop, P. Discovery of a novel, potent, and specific family of factor Xa inhibitors via combinatorial chemistry. *Biochemistry* **1998**, *37*, 1053–1059. The K_i values were averaged from triplicate determination, and the standard deviation of the positive control was <15% of the mean.
- (16) (a) Joule, J. A. Product class 13: indole and its derivatives. *Sci. Synth.* **2001**, *10*, 361–652. (b) Gribble, G. W. Recent developments in indole ring synthesis—methodology and applications. *J. Chem. Soc., Perkin Trans. 1* **2000**, 1045–1075.
- (17) (a) Chen, C.-Y.; Lieberman, D. R.; Larsen, R. D.; Verhoeven, T. R.; Reider, P. J. Syntheses of indoles via a palladium-catalyzed annulation between iodoanilines and ketones. *J. Org. Chem.* **1997**, *62*, 2676–2677. (b) Nazaré, M.; Schneider, C.; Lindenschmidt, A.; Will, D. W. A flexible, palladium-catalyzed indole and azaindole synthesis by direct annulation of chloroanilines and chloroaminopyridines with ketones. *Angew. Chem, Int. Ed.* **2004**, *43*, 4526–4528.
- (18) Matter, H.; Defossa, E.; Heinelt, U.; Blohm, P.-M.; Schneider, D.; Mueller, A.; Herok, S.; Schreuder, H.; Liesum, A.; Brachvogel, V.; Loenze, P.; Walser, A.; Al-Obeidi, F.; Wildgoose, P. Design and quantitative structure–activity relationship of 3-amidinobenzyl-1H-indole-2-carboxamides as potent, nonchiral, and selective inhibitors of blood coagulation factor Xa. *J. Med. Chem.* **2002**, *45*, 2749–2769.
- (19) Tucker, T. J.; Brady, S. F.; Lumma, W. C.; Lewis, S. D.; Gardell, S. J.; Naylor-Olsen, A. M.; Yan, Y.; Sisko, J. T.; Stauffer, K. J.; Lucas, B. J.; Lynch, J. J.; Cook, J. J.; Stranieri, M. T.; Holahan, M. A.; Lyle, E. A.; Baskin, E. P.; Chen, I. W.; Dancheck, K. B.; Krueger, J. A.; Cooper, C. M.; Vacca, J. P. Design and synthesis of a series of potent and orally bioavailable noncovalent thrombin inhibitors that utilize nonbasic groups in the P1 position. *J. Med. Chem.* **1998**, *41*, 3210–3219.
- (20) Kabsch, W. Evaluation of single-crystal X-ray diffraction data from a position sensitive detector. *J. Appl. Crystallogr.* **1988**, *21*, 916–924.
- (21) Brünger, A. T. *X-PLOR: A System for X-ray Crystallography and NMR*, version 3.1; Yale University Press: New Haven, CT, 1992.
- (22) PDB files from RSCB Protein Database: <http://www.rcsb.org/pdb>. (a) Bernstein, F. C.; Koetzle, T. F.; Williams, G. J. B.; Meyer, E. F.; Brice, M. D.; Rodgers, J. R.; Kennard, O.; Shimanouchi, T.; Tasumi, M. The protein data bank: a computer-based archival file for macromolecular structures. *J. Mol. Biol.* **1977**, *112*, 535–542. (b) Berman, J. W.; Zukang, F.; Gilliland, G.; Bhat, T. N.; Weissig, H.; Shindyalov, I. N.; Bourne, P. E. The protein data bank. *Nucleic Acids Res.* **2000**, *28*, 235–242.
- (23) Goodford, P. J. A computational procedure for determining energetically favorable binding sites on biologically important macromolecules. *J. Med. Chem.* **1985**, *28*, 849–857.
- (24) McMartin, C.; Bohacek, R. S. QXP: powerful, rapid computer algorithms for structure-based drug design. *J. Comput.-Aided Mol. Des.* **1997**, *11*, 333–344.
- (25) Weiner, S. J.; Kollman, P. A.; Case, D. A.; Singh, U. C.; Ghio, C.; Algona, G.; Profeta, S.; Weiner, P. A new force field for molecular mechanical simulation of nucleic acids and proteins. *J. Am. Chem. Soc.* **1984**, *106*, 765–784.
- (26) (a) Halgren, T. Maximally diagonal force constants in dependent angle-bending coordinates. II. Implications for the design of empirical force fields. *J. Am. Chem. Soc.* **1990**, *112*, 4710–4723. (b) Halgren, T. MMFF VI. MMFF94s option for energy minimization studies. *J. Comput. Chem.* **1999**, *20*, 720–729.
- (27) SYBYL Molecular Modelling Package, version 6.9; Tripos: St. Louis, MO, 2003.
- (28) (a) Heiden, W.; Goetze, T.; Brickmann, J. Fast generation of molecular surfaces from 3D data fields with enhanced “marching cube” algorithm. *J. Comput. Chem.* **1993**, *14*, 246–250. (b) Brickmann, J.; Bertling, H.; Bussian, B. M.; Goetze, T.; Knoblauch, M.; Waldherr-Teschner, M. MOLCAD—interactive molecular computer graphics on high-performance computers. *Tagungsber.-Vortragstag., Ges. Dtsch. Chem., Fachgruppe Chem.-Inf.* **1987**, 93–111.
- (29) Heiden, W.; Moeckel, G.; Brickmann, J. A new approach to the display of local lipophilicity/hydrophilicity mapped on molecular surfaces. *J. Comput.-Aided Mol. Des.* **1993**, *7*, 503–514.
- (30) (a) Ghose, A.; Crippen, G. Atomic physicochemical parameters for three-dimensional structure-directed quantitative structure–activity relationships. 1. Partition coefficients as a measure of hydrophobicity. *J. Comput. Chem.* **1986**, *7*, 565–577. (b) Viswanadhan, V. N.; Ghose, A. K.; Revankar, G. R.; Robins, R. K. Atomic physicochemical parameters for three-dimensional structure-directed quantitative structure–activity relationships. 4. Additional parameters for hydrophobic and dispersive interactions and their application for an automated superposition of certain naturally occurring nucleoside antibiotics. *J. Chem. Inf. Comput. Sci.* **1989**, *29*, 163–172.
- (31) (a) Connolly, M. L. Solvent-accessible surfaces of proteins and nucleic acids. *Science* **1983**, *221*, 709–713. (b) Connolly, M. L. Analytical molecular surface calculation. *J. Appl. Crystallogr.* **1983**, *16*, 548–558.

JM0490540